INSTITUTE OF PHYSICS PUBLISHING REPORTS ON PROGRESS IN PHYSICS

Rep. Prog. Phys. **66** (2003) 1045–1094 PII: S0034-4885(03)55948-6

Trends in high energy particle accelerators

S Tazzari[1] **and M Ferrario**[2]

[1]Viale della Ricerca Scientifica 1, Universita di Roma, 00173 Roma, Italy
[2]INFN-LNF, Via E. Fermi 40, 00044 Frascati, Italy

Received 12 November 2002
Published 21 May 2003
Online at stacks.iop.org/RoPP/66/1045

Abstract

Particle accelerators of higher and higher energy and intensity are required, as the investigation of subatomic matter needs to be pursued with higher and higher resolving power. To keep pace with this need while keeping physical dimensions and the cost of accelerator installations affordable, ever new ideas and technologies must be devised. After a brief general introduction and a summary of accelerator physics basics, we review the main lines of development of state of the art installations recently built, in construction or on the drafting board. New physics and technology challenges they pose and main topics still open to further research and development are also outlined.

Contents

1. Introduction

1.1. General

It has been elegantly said that 'the burning problems of today's particle physics are: mass, flavour and unification' [1] or, in other words [2], electro-weak symmetry breaking and new physics, the Universe composition (one kind of matter only) and its origin, the neutrino puzzles (missing solar electron neutrinos and atmospheric e to μ neutrino ratio, some aspects of which have been clarified since being started). High energy (HE) particle accelerators, producing particle beams to 'illuminate' subatomic matter, are the tools to investigate them.

Viewed as microscopes, their resolving power is inversely proportional to the accelerated particle de Broglie wavelength $\lambda = \hbar c/E$: the higher the energy the higher the resolving power. On the other hand, beam energy can be converted into mass to create new particles and quanta, whether predicted or unexpected. The higher their mass the higher the needed beam energy.

The major breakthrough in the strive towards ever higher energies has been made by machines (colliders) designed to collide head-on particle beams of same or comparable energies travelling in opposite directions. Because in a head-on collision between equal energy beams of identical particles the energy freed in the centre of mass (c.m.) reference system scales linearly with beam energy rather than with its square root as in the case when the target particles are at rest, for given $E_{\text{c.m.}}$ the needed colliding beams energy is 2γ times lower than in the fixed target case, γ being the accelerated particles Lorentz factor. At high $E_{\text{c.m.}}$ the factor can become extremely large, the lighter the particle the larger the factor: for LEP, the CERN 200 GeV c.m. e^+e^- collider, $2\gamma \approx 4 \times 10^5$ while for a 200 GeV c.m. pp collider $2\gamma \approx 4 \times 10^2$. All this had been realized early in the past century but not until the mid 1950s had accelerator technology progressed enough to allow the first pioneering installations, based on circular accelerators, to be built [3]. Not surprisingly, all highest energy accelerators, present and planned, are nowadays colliding beam devices.

Both scope and technology of accelerators depend on the kind of accelerated particle. As for scope, hadron and lepton colliders are the tools to address the mass problem by exploring the physics beyond the standard model (Higgs field, super symmetries, string and super string theories) [4]. Hadron colliders with energies in the tens to hundreds of TeV range, providing sub-quark-size resolution of less than 10^{-18} cm, are honed to maximum potential for new discoveries. Complementary lepton colliders produce elementary point like collisions and clean final states to perform refined measurements of newly found phenomena. With LEP (e^+e^-, 200 GeV c.m.) having closed down at the end of 2000, the highest energy accelerator is the 1 TeV FNAL Tevatron $\bar{p}p$ collider, undergoing important upgrades. The first next generation pp, 14 TeV c.m. hadron collider, LHC, is in construction at CERN in the 27 km long LEP tunnel [5].

More specialized ep colliders are used to explore the inner structure of hadrons by taking advantage of the point-like, elementary nature of the electron and of the possibility of obtaining significant polarization. The 27.5/920 GeV only ep collider HERA is in operation in Hamburg at DESY and is also being significantly upgraded [6].

Much higher energy densities are demanded to attack cosmological problems by gaining information on the state of primeval matter. Ultra-relativistic energy ion–ion collisions of nuclei as heavy as lead or gold produce GeV/f^3 energy densities and temperatures in the 10^{12} K range, such that phase transitions from hadronic matter to a confined plasma of quarks and gluons, the early state of the universe, can be studied [7]. Following fixed target experiments with the CERN SpS, 160 GeV A^{-1} lead ion beam, the first dedicated ion–ion collider, the

210 GeV A^{-1} RHIC, has come into operation in 2001 at BNL [8] and has produced the first physics results [9].

But energy is only one side of the picture, the event rate of the reactions to be studied being the other. The event rate per unit cross-section and per crossing point, L, independent of the reaction, is called luminosity. It is usually measured in $(\mathrm{nb\,s})^{-1}$, corresponding to $10^{33}\,\mathrm{cm}^{-2}\,\mathrm{s}^{-1}$. High peak and average luminosities are prime collider requirements and, because point-like cross-sections scale like $1/E^2$, luminosity should ideally scale at least accordingly.

When trains of rigid bunches each containing N_b particles, having the same effective transverse cross-section area S^* at the interaction (collision) point (IP) and overlapping perfectly, collide head-on at a rate f, the general expression for luminosity is

$$L = f \cdot N_\mathrm{b} \cdot \left(\frac{N_\mathrm{b}}{S^*}\right), \tag{1.1.1}$$

proportional to the particle density in transverse space. The keys to high luminosity are thus high bunch charge and small cross-section.

e^+e^- colliders at relatively low c.m. energies but with very high luminosity, the 'meson factories', are needed to attack the matter–antimatter problem. By producing great quantities of Φ, K and B mesons they allow precision measurements of CP violations through the study of meson pair decays. Tau meson factory designs are still on the drafting board.

Finally, neutrino physics is today studied in the laboratory using neutrino beams generated by bombarding a fixed target with p beams produced by high power, relatively low energy proton accelerators. Neutrino factories, to provide significantly higher intensity ν beams, are being studied for a next step.

It may be worth recalling that, while being in number only less than a per cent of all particle accelerators in operation world wide, HE machines forge—so to speak—the future: new trends and technologies developed for them spill over into a multitude of other accelerator applications.

1.2. The next generation

Physics at the energy frontier will rest on the FNAL Tevatron and on HERA until ≈2006–2007 when LHC, in construction at CERN, is scheduled to start doing physics. There is general consensus in the physics community on the fact that an e^+e^- collider with c.m. energy ≈0.4 TeV should be built early enough to provide significant time overlap with the LHC and that solid R&D programs should also be maintained, in preparation for a farther future, on very large hadron colliders (VLHC) with energy ⩾100 TeV, on 3–5 TeV e^+e^- linear colliders (CLIC), on neutrino factories and on heavy lepton colliders.

All present generation frontier accelerators, with the only exception of the Stanford linear collider (SLC) [10], are circular machines. The scheme, still valid for next generation pp and heavy ion accelerators, encounters severe difficulties in being extended to significantly higher electron energies because particles constrained on curved orbits radiate energy away in proportion to γ^4. Other schemes are therefore being proposed: e^+e^- face-to-face linear accelerators (linear colliders (LCs)) or circular machines to accelerate the much heavier muon (muon colliders). The latter is an attractive alternative because of its compactness and energy reach potential but, since production and acceleration of intense beams of short lived particles poses severe technical challenges, its feasibility is still being studied and researched.

Significant near future upgrades of meson factories to much higher luminosity are being planned. The feasibility of muon storage ring based neutrino factories [11], an intermediate step towards muon colliders, is also being actively investigated.

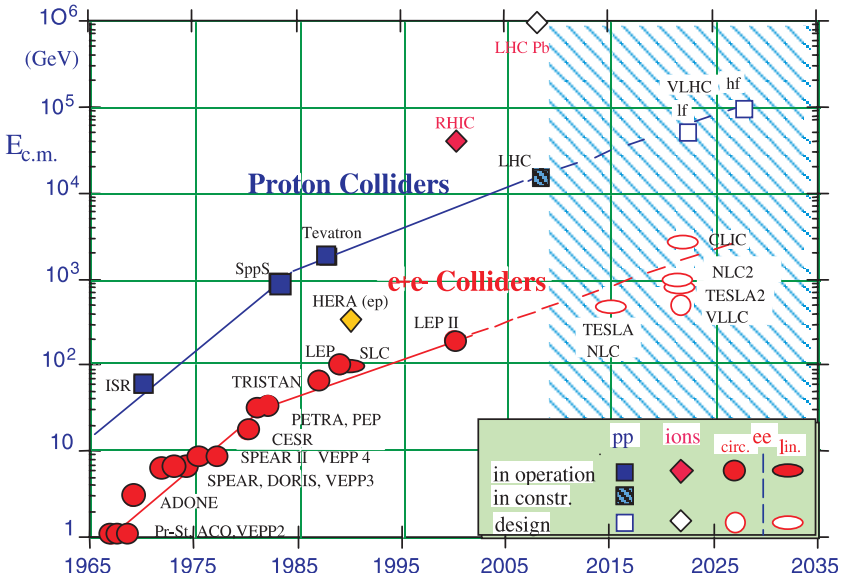

Figure 1. Possible evolution of the highest energy proton, ion and electron colliders. Project dates are those of completion; in the dashed area they are only tentative.

The future of both heavy ion and *ep* colliders is planned either through upgrades of existing installations or by including the capability for ion and *ep* collisions as options in the design of new *pp* machines.

Finally, exotic linear acceleration schemes to achieve extremely high accelerating fields are also being studied for an even farther future.

Past history and future prospects of proton and electron collider energies are schematically shown in figure 1.

2. Circular colliders

2.1. General description

In a typical circular collider scheme two counter rotating beams, each consisting of a train of n_b equally spaced bunches, are injected in either the same or in two separate rings, accelerated to their final operating energy E and kept coasting. Very schematically, the ring magnetic lattice layout defines the ideal (reference) particle orbit—lying in the horizontal plane and along which a coordinate s is defined—followed by a particle having nominal energy and initial conditions. The orbit is made of arcs connecting long straight sections where detectors, injection equipment, accelerating RF cavities and other auxiliaries are installed. The magnetic lattice main elements are bending and focusing magnets with fields transverse to the trajectory. Special focusing is provided in the straight interaction regions (IRs) where collisions take place. Bending radius ρ_0, particle energy E and bending magnetic field B obey the well-known equation

$$P \approx \frac{E}{c} = qB\rho_0. \tag{2.1.1}$$

In a paraxial, linear approximation particles can be shown to perform betatron oscillations around the reference orbit, independently along two orthogonal x (radial) and z (vertical)

directions perpendicular to the orbit itself, within beam envelopes that define the local transverse beam sizes. The numbers of oscillation periods per revolution, $Q_{x,z}$, are defined by the lattice and called lattice tunes. Whenever particles are only subject to the system of external, conservative forces produced by the lattice, the areas ε_{nx} and ε_{nz} occupied by the beam in the (x, p_x), (z, p_z) transverse phase planes respectively are invariants of motion (invariant emittances). Beam transverse sizes at collision points are given by

$$\sqrt{\varepsilon_{x,z} \cdot \beta_{x,z}(s)} \qquad \text{with } \varepsilon_{x,z} = \frac{\varepsilon_{nx,nz}}{\gamma} \text{ (beam emittances).} \tag{2.1.2}$$

$\beta_x(s)$, $\beta_z(s)$ (radial and vertical beta functions) are single valued, periodic envelope functions characteristic of the lattice. Besides modulating the transverse beam sizes, the β functions have the important property that any perturbation to the particle trajectory applied at the abscissa s_0 produces, at s, an effect that scales like $\sqrt{\beta(s_0) \cdot \beta(s)}$. Finally, in the field free region next to a beam waist located at s_0, one has

$$\beta(s) = \beta(s_0) + \frac{s^2}{\beta(s_0)} \tag{2.1.3}$$

showing that $\beta(s_0)$ is the waist Rayleigh length.

Because a circular machine lattice is necessarily periodic, any (inevitably present) perturbation becomes resonant with the particle revolution frequency whenever a linear combinations of tunes $mQ_x + nQ_z$—with m, n positive integers and $(m + n)$ called the resonance order—adds up to an integer. The resonance strength decreases with increasing order: low order resonances may cause beam loss or blow-up and must be avoided.

Beams are accelerated by sinusoidal electric fields parallel to the reference trajectory. Particles within a given energy spread around the nominal energy are captured in the field potential wells (buckets) in which they oscillate longitudinally, along s. The beam is thus bunched, the longitudinal oscillation envelope defining the bunch length.

During injection and acceleration collisions must not occur and the beams must be kept everywhere apart (section 2.2). They are brought together, when coasting, only within specially designed straight IRs, at N_{IP} IPs around which the detectors are laid out. When circulating bunches are few and far apart like in LEP, opposite charge beams travelling in a same vacuum chamber can be separated by means of electric fields [12]. When operating with many, closely spaced bunches, two separate chambers everywhere other than in the IRs become mandatory and to achieve separation as close as possible to the IP, beams are usually made to cross at an angle. The IR magnetic optics, designed to bring the beams to a sharp focus (low β values) at the IP, requires strong and well compensated, large aperture quadrupolar lenses. Beam conditions at the IPs and in the IRs, in particular collision processes and other beam generated events, also affect the detector by producing backgrounds whose control and minimization sets technical constraints on the collider design as a whole. The design of the IR optics is therefore a challenging task.

Injection and acceleration are usually quite lengthy and delicate procedures. It is therefore desirable for the beams to be kept stored and colliding for as long as possible. There are several lifetime limiting mechanisms by which particles can be lost from the beam, such as scattering and bremsstrahlung on the residual gas, radiation, decay, neutralization and beam–beam interactions themselves. Intra-beam scattering and other diffusion mechanisms that gradually blow-up the beam emittance may also define 'useful' lifetimes by loss, if not of particles, of luminosity.

Finally, as mentioned earlier, radiation may have considerable influence on beam dynamics and collider technology. It sets practical limits on the top energy of fully radiation dominated machines such as HE circular electron colliders and does also affect the design of next

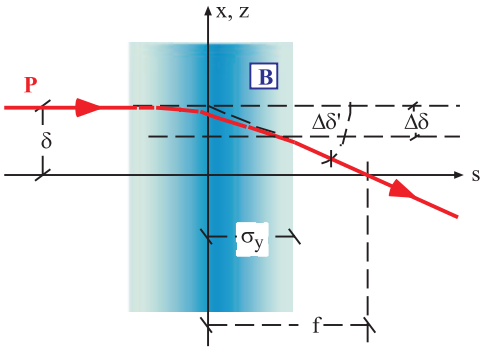

Figure 2. Particle P deflected by a bunch B with rms length σ_y and infinite transverse dimensions.

generation proton colliders. Radiation losses make the system non-conservative and the normalized beam emittance no longer invariant. They also cause the number of stored particles to decay exponentially with time constant τ_{rad}. On the other hand they have the beneficial effect of damping particle betatron and energy oscillations, and therefore beam sizes, to final equilibrium values, with time constants τ_x, τ_z, τ_E scaling for a given lattice like γ^{-3}. One normally has $\tau_x = \tau_z = 2\tau_E$.

On the technical side, the fraction of beam energy radiated away at each revolution has to be replenished by the accelerating system, which makes the latter the most critical and most expensive items of a HE electron collider. The accelerator vacuum system must also deal with the overall radiated power and power density that create thermal loads and induce gas desorption from the vacuum chamber walls.

2.2. *Luminosity and beam–beam limit*

With n_{b} Gaussian bunches uniformly spaced by $d = C/n_{\text{b}}$ around the circumference C, one obtains from equation (1.1.1):

$$L = \frac{c}{d} \cdot N_{\text{b}} \cdot \left(\frac{N_{\text{b}}}{S^*}\right), \qquad \text{with } S^* = 4\pi(\sigma_x^*\sigma_z^*) \equiv 4\pi \cdot r \cdot \sigma_x^{*2}, \tag{2.2.1}$$

$\sigma_{x,z}^*$ being the bunch rms transverse dimensions, and $r \equiv \sigma_z^*/\sigma_x^*$ the ratio of vertical to horizontal bunch size[1]. A limit to the maximum achievable L arises from beam–beam interaction effects that limit the maximum achievable particle density (N_{b}/S^*). In fact, particles of one bunch travelling at a distance $\delta \neq 0$ from the reference trajectory are deflected in the electromagnetic field of the other bunch (figure 2); in a paraxial, linear approximation $(\delta \ll \sigma_x^*, \sigma_z^*)$ the bunch charge distribution acts like a thin lens, focusing in both planes, with radial and vertical focal lengths f_x, f_z, given by

$$\begin{vmatrix} f_x \\ f_z \end{vmatrix} = \gamma \cdot \left(\frac{1+r}{2r_0} \cdot \frac{S^*}{N_{\text{b}}}\right) \cdot \begin{vmatrix} 1/r \\ 1 \end{vmatrix}, \tag{2.2.2}$$

r_0 being the particle classical radius.

It can be shown that particle tunes are consequently shifted by

$$\begin{vmatrix} \Delta Q_x \\ \Delta Q_z \end{vmatrix} \approx \begin{vmatrix} \xi_x \\ \xi_z \end{vmatrix} = \frac{1}{\gamma}\left[\frac{r_0}{2\pi} \cdot \left(\frac{N_{\text{b}}}{\sigma_x^*\sigma_z^*}\right) \cdot \left(\frac{1}{1+r}\right)\right] \begin{vmatrix} \beta_x^* \cdot r \\ \beta_z^* \end{vmatrix}. \tag{2.2.3}$$

[1] Asterisks always indicate parameter values at the IP.

From figure 2 and from equation (2.2.2) and (2.2.3) the following equalities can also be derived:

$$f_{x,z} = \frac{\beta^*_{x,z}}{4\pi\xi_{x,z}} \approx \frac{\sigma_y}{|\Delta\delta/\delta|_{x,z}} \equiv \frac{\sigma_y}{D_{x,z}}. \tag{2.2.4}$$

$D_{x,z} \equiv |\Delta\delta/\delta|_{x,z}$ being called disruption factor (section 3.1.2). In circular colliders, for beams to survive the interaction $D_{x,z}$ must be $\lessapprox 1$, so that $f_{x,z} \gtrapprox \sigma_y$.

When one now takes into account the spread in particle oscillation amplitudes and the non-linearity of the space charge force, one sees that the interaction actually generates a particle dependent tune shift and therefore an incoherent tune spread $0 \leqslant \Delta Q_{x,z} \leqslant \xi_{x,z}$ covering a finite area 'footprint' in the Q_x, Q_z tune plane. A simulation of the CERN LHC tune spread footprint at nominal luminosity is shown, as an example, in figure 13. A limit to the tolerable maximum tune spread, $\xi_{\rm lim}$, in either of the two planes is thus defined by the tune footprint starting to overlap dangerous resonance lines, causing beams to blow-up and luminosity to drop.

To fully maximize L one usually makes $\xi_x = \xi_z$ by letting $r = \beta^*_z/\beta^*_x$ in which case, expressing L as a function of ξ_z, one obtains the simple formula

$$L = \frac{c}{2r_0} \cdot \left(\frac{N_{\rm b}}{d}\right) \cdot (1+r) \cdot \frac{\xi_z \gamma}{\beta^*_z}. \tag{2.2.5}$$

The actual situation is more complicated than described by the model because bunches are not rigid. Equation (2.2.5) is therefore normally used to determine $\xi_{\rm lim}$ from experiment. Values found are in the range $\xi_{\rm lim} \approx 0.04$–$0.08$ for electrons and $\xi_{\rm lim} \approx 0.005$–$0.009$ for protons [13], the limit being less stringent for light than for heavy particles because of high order resonances being damped by radiation. To extrapolate these values to different energies a simple scaling law for $\xi_{\rm lim}$ has been originally proposed in [14], based on the assumption that, since betatron oscillations are radiation damped with time constant τ_β, a parameter relevant to the perturbation induced by the interaction must be the number of interactions in a damping time, n_τ, or rather its inverse, the damping decrement in between successive crossings $\delta \approx 1/n_\tau$. Existing experimental data and recent simulations on both proton and electron colliders are rather well fitted by a saturating power law of the form

$$\xi_{\rm lim} = a + b \cdot \delta^\alpha \qquad \text{with } \tfrac{1}{3} \lessapprox \alpha \lessapprox \tfrac{1}{2} \tag{2.2.6}$$

Two examples of such a fit, including values of $\xi_{\rm lim}$ assumed for future e^+e^- and pp collider designs are shown in figure 3, compared to numerical tracking through many turns of bunches modelled as ensembles of a manageable number of 'macroparticles' [15].

Schemes to compensate the space charge effect have been proposed at various times and tested at e^+e^- colliders DCI and VEPP-4 but none has succeeded in significantly raising L.

Equations (2.2.5) and (2.2.3) respectively show that, to maximize L, β^*_z must be minimized and that the limit on ξ imposes preventing crossings where $\beta_{x,z} > \beta^*_{x,z}$.

Several effects contribute to defining the minimum tolerable β^*_z value. One is that, according to equation (2.1.3), the lower the β^* the higher β becomes inside the nearest IR focusing lenses. As an example, the LEP IR configuration [12] has $\beta_{\rm max}/\beta^* \approx 2500$, corresponding to a $\sigma_{z\,\rm max}/\sigma^*_z$ ratio of $\approx$50. A large β at the lenses imposes large lens apertures and enhances the effect of any field error, resulting in optics aberrations and resonance excitation. Large beam sizes in the vicinity of detectors also cause more particles to be lost locally resulting in increased backgrounds. On the other hand making β^* smaller than approximately twice the bunch length is of no use since particles at the head and the tail of the bunch, that do not collide exactly at the IP, would see values of β larger than β^* causing the local value of $\xi_{\rm lim}$ to be exceeded.

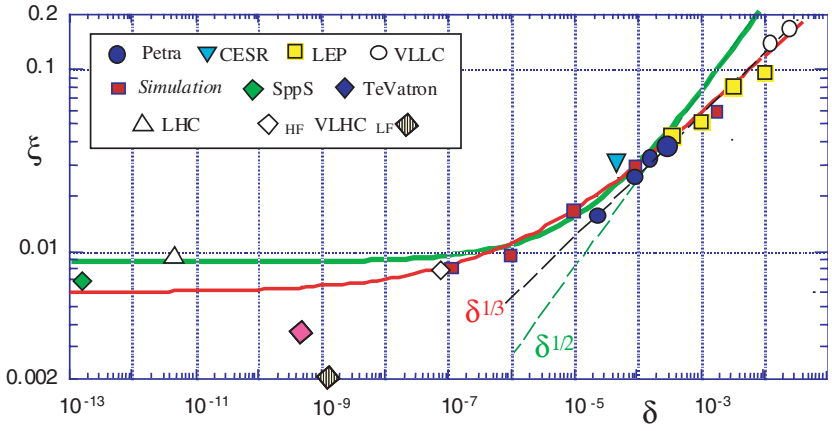

Figure 3. $\xi_{\rm lim}$ as a function of the 'damping decrement' factor. LHC and VLHC data are nominal design values.

For given ξ, one gains on L by increasing the beam emittance and $N_{\rm b}$ while keeping $N_{\rm b}/S^*$ constant. But again, larger beam sizes require larger, more expensive vacuum chamber and magnet apertures.

Coming back to equation (2.2.5), the lowest value of d, or the largest number of circulating bunches, is limited by the distance needed to properly separate neighbouring bunches away from the IP and, like the maximum value of $N_{\rm b}$, ultimately by single and multibunch instabilities of various nature, particularly at injection energy. In weakly radiating hadron colliders d is usually pushed to its lower limit, determined by bunch separation being large enough to minimize the effect of transverse, mostly coherent, non-linear, long-range beam–beam forces as bunches go by each other [16] (see section 2.3.2). As mentioned earlier, crossing angles

$$\theta_{x,z} \lessapprox \frac{\sigma_{x,z}}{\sigma_y} \tag{2.2.7}$$

are also usually utilized for faster separation.

Ultimate boundaries to the maximum value of $n_{\rm b}N_{\rm b}$ (proportional to $N_{\rm b}/d$) may finally be set by the maximum number of events per bunch crossing the detectors can resolve and, for radiation dominated machines, by technical or cost considerations limiting the overall machine power consumption.

2.2.1. e^+e^- colliders. HE circular electron colliders are radiation dominated. Beam emittance, bunch size and beam energy spread are thus uniquely determined by the ring lattice and by beam dynamics in the presence of radiation. As mentioned earlier, they result from equilibrium between exponential damping and diffusion-like anti-damping, the radial and vertical betatron emittances being damped towards finite equilibrium values $\varepsilon_x \gg \varepsilon_z$, which for a given lattice scale like γ^2. Radiation dominated beams are thus normally ribbon-like, with $r = \sigma_z/\sigma_x \ll 1$. The beam relative momentum spread at equilibrium is

$$\sigma_{\rm p} \propto \gamma \cdot \rho_0^{-1/2}. \tag{2.2.8}$$

At each turn each particle radiates away, on average, an energy U_0, given by

$$U_0 = C_{\gamma n}\frac{\gamma^4}{\rho_0} \qquad \text{with } C_{\gamma n} = 6.08\,\text{GeV m}. \tag{2.2.9}$$

The accelerating RF voltage, $V = (U_0/q)$, required to turn by turn replace the lost energy, is proportional to γ^4/ρ_0 while the needed peak RF voltage is $\hat{V} = a_{\rm ov} \cdot V$, the overvoltage factor $a_{\rm ov} > 1$ providing a deep enough RF bucket for the lifetime from stochastic energy fluctuations spilling particles out to be sufficiently long.

The total radiated power for a beam current $i = q f_0 n_{\rm b} N_{\rm b}$ is $P_{\rm B} = i \cdot U_0 \propto i \cdot \gamma^4/\rho_0$ and the corresponding overall RF power needed, including that ($P_{\rm D}$) dissipated in the accelerating structure, is

$$P_{\rm RF} = 2(P_{\rm B} + P_{\rm D}) \propto \left(\frac{i\gamma^4}{\rho_0}\right) \cdot \left[1 + C_\Omega \cdot a_{\rm ov}^2 \left(\frac{i\gamma^4}{Q\rho_0}\right)\right]. \tag{2.2.10}$$

Here Q is the RF resonators (cavities) quality factor, C_Ω is a coefficient depending on the cavity type and the factor of 2 accounts for the two beams.

The dependence of $P_{\rm RF}$ on energy to very large exponents not only puts a sharp limit on the uppermost energy and current of a given machine but also definitely limits the energy at which electron colliders are feasible and economically affordable, particularly when L and E must increase in parallel. LEP, requiring $V \gtrapprox 3\,\text{GV}$, $a_{\rm ov} \approx 1.4$ and $P_{\rm RF} \gtrapprox 14\,\text{MW}$, is considered having come close to the cost to performance ratio upper limit.

Technically, because, for given cavity shape, accelerating voltage and beam current, the efficiency $\eta_{\rm RF} = P_{\rm B}/(P_{\rm B} + P_{\rm D})$ of energy transfer to the beam only depends on the structure quality factor Q, the needs of electron colliders have stimulated an impressive amount of R&D work on the development of superconducting accelerating RF systems, performed in a collaborative way by laboratories and Universities in Europe, USA and Japan. This because the Q of superconducting RF systems can be a factor of 10^5–10^6 higher than that of room temperature ones, a gain only partially offset, power consumption wise, by the Carnot efficiency factor of order $\approx 10^{-3}$ involved in removing power at cryogenic temperatures. High efficiency minimizes operating cost or, for the same cost, allows higher beam power and CW operation.

Pioneering work was done at CERN where the Nb coated copper cavity system, developed and installed on LEP [17], has made it possible to reach and exceed the 100 GeV design beam energy. A comparison between the initial warm RF system of LEPs first stage and the final cold one is shown in table 1.

Progress in the peak field of operational superconducting resonators is shown in figure 27 and reviewed in [18].

2.2.2. Design trends. An empirical approximate rule, since long worked out to minimize the overall cost of electron colliders, dictates that the bending magnet radius should increase

Table 1. Efficiencies and power requirements of the LEP RF cavities.

LEP RF system	Cu (warm)	Nb (4.2 K)
Frequency (MHz)	350	350
Accelerating field (MV m^{-1})	1.5	7.5
Active length (m)	2.13	1.7
Iris hole diameter (mm)	100	241
Q	4.E+04	4.E+09
Dissipated power per metre (KW m^{-1})	43	2.5E−02
Dissipated power per MV ($P_{\rm MV}$) (KW MV^{-1})	29	3.3E−03
$P_{\rm MV}$(Cu)/$P_{\rm MV}$(Nb)[a]	20	
Nb/Cu stored energy/m ratio		39

[a] Refrigeration efficiency and static losses included.

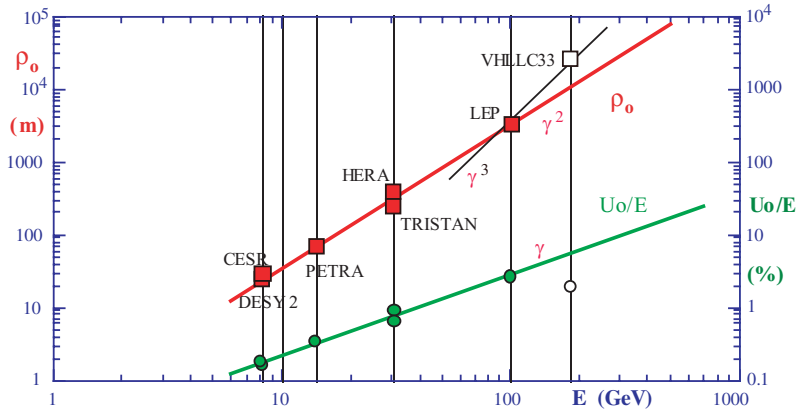

Figure 4. HE e^+e^- colliders. Bending radius and fraction of energy lost per turn vs top energy.

proportional to the square of the energy. The cost resulting from the $\rho_0 \propto \gamma^2$ rule is also roughly proportional to γ^2 while the exponents of γ in equation (2.2.10), are divided by two. According to equation (2.2.8) the rule also produces an energy independent relative momentum spread.

Figure 4, in which ρ_0 and the ratio U_0/E of radiated energy per turn to nominal energy are plotted as functions of the nominal energy (per beam) of the highest energy circular e^+e^- machines in operation, shows that the rule has been so far followed to good approximation. An obvious ultimate limit for the energy eventually derives, as shown by figure 4, from either the circumference length or from $U_0(E_{\max})$ becoming too large a fraction of $E_{\max}$.

As for luminosity, equation (2.2.5), re-written as

$$L = \frac{\rho_0}{4C_{\gamma n} r_0} \cdot \frac{\xi}{\beta_z^*} \cdot \frac{P_B}{\gamma^3} \qquad \text{with } C_{\gamma n} = 6.03 \times 10^{-16}\,\text{cm GeV} \tag{2.2.11}$$

to evidence the dependence on beam power P_B, shows that by the above rule P_B must scale like γ, even at constant L. If instead P_B, for reasons of cost and social impact, the overall power consumption of present large facilities amounting to hundreds of MW, must not be much exceeded, ρ_0 should scale rather like γ^3, soon leading to impractically large radii.

The solution to turn to LCs, for which radiation is totally negligible, was identified quite early [19, 20]. Because their cost is proportional to energy a break-even energy exists above which a circular machine is no longer the less expensive choice. The first (almost) LC, SLC [9], has been in operation at SLAC for a number of years and several proposals to build much higher energy ones have been put forward and are being actively developed; they are discussed in section 3.

Lately however a new interest in circular collider energies higher than LEP has been raised by the fact that tunnels with circumferences upwards of 200 km are being proposed to house a very large hadron collider (VLHC) with c.m. energy in excess of 100 TeV (section 2.3). The availability 'for free' of such a tunnel with its general purpose services, prompts to investigate the feasibility of a very large lepton collider (VLLC) housed in the same tunnel—next to or on top of the VLHC and possibly using the same injector chain—in the expectation that its marginal cost would be comparatively low. Table 2 lists the parameters of a design called VLLC-33 based on the above criteria [21].

The double ring, single IR machine circumference is 233 km, with a 25.9 km bending radius. The design is optimized for this circumference and bending radius and for fixed total

Table 2. LEP and VLLC main parameters.

Parameter	Units	LEP	VLLC-33
Beam energy	GeV	100	186
Circumference	Km	26.7	233
Number of interaction points		4	1
Luminosity	$(\text{nb s})^{-1}$	0.03	0.1
β_x^*/β_z^*	cm	150/5	100/1
Emittances e_x/e_z	nm	21.1/0.2	3.1/0.03
RMS beam size at IP σ_x/σ_z	mm	178/3.3	56/06
Beam–beam tune shift ξ_x/ξ_z		0.04/0.08	0.2/0.2
Bunch length	mm	11	6.7
Beam rms energy spread	%	0.45	0.1
Particles per bunch	10^{11}	4.0	4.9
Number of bunches per beam		4	114
Bunch spacing	km	6.70	2.00
Total beam current (two beams)	mA	5.8	22.8
Stored beam energy	MJ	0.03	1.66
e^+e^- bremmstrahlung lifetime	h	6	5
Dipole field at top energy	T	0.11	0.021
Energy loss per turn, U_0	GeV	2.67	4.42
Critical energy	keV	686	515
Synchrotron radiated power (two beams)	MW	14.5	100.7
Power load from both beams	kW m^{-1}	0.82	0.46
Longitudinal damping time	turns	73	45
RF frequency	MHz	352.21	400
RF voltage	GV	3.05	4.85
Available RF power	MW	34.1	(−150)

(two beams) radiated power of $P_\text{B} = 100$ MW. The resulting c.m. energy is 372 GeV. The power is about a factor of 7 higher than the LEP one and, even with the best present wall-plug to beam efficiency of large superconducting RF systems, would correspond to an overall RF system power consumption of ≈400 MW. The required RF voltage is obtained from $\hat{V} = a_\text{ov} \cdot (U_0/q)$ with $a_\text{ov} = 1.17$ and the storable current from $i = U_0/P_\text{B}$. The limit value of L is derived from equation (2.2.11) as

$$L_\text{lim} \cdot \gamma^3 = \frac{\rho_0 P_\text{B}}{4 C_{\gamma n} r_0} \cdot \frac{\xi_\text{lim}(\gamma)}{\beta_z^*}, \tag{2.2.12}$$

evidencing that, provided that number of bunches and bunch sizes can be adjusted so as to reach ξ_lim, the only remaining free parameter controlling $L \cdot \gamma^3$ is β_z^*. Other hidden constraints though exist, such as the maximum RF voltage one is prepared to provide, the maximum current storable at injection, the minimum allowed ratio between injection energy and operating energy, etc. The VLLC proposed parameters are compared to LEP ones in table 2.

To maximize L, the design assumes that ξ_lim can be scaled according to a model very close to that of equation (2.2.6) to a value 1.5 times higher than LEPs and that β_z^* can be lowered, with respect to LEP, by a factor of 5, which allows gaining almost two orders of magnitude in nominal L. The proposed superconducting RF system is similar to and only ≈30% longer than the LEP one and should not give problems except for having to be divided into a number of subsystems more or less evenly distributed along the 220 km circumference, in order to keep the beam energy sufficiently constant over a turn.

A number of technical challenges are to be faced. The top energy dipole field is comparable to LEP's injection one, meaning that even for the same top to injection energy ratio, requiring

a 40 GeV injector, it remains an open question whether at injection energy the typical relative field error tolerance of $\approx 10^{-4}$, corresponding to absolute field errors two orders of magnitude lower than the earth magnetic field, can be kept.

Another issue to be addressed is the design of a very long, UHV vacuum chamber with low enough impedance and able to sustain a large radiation power load which, up to $\approx$100 GeV, is mostly dissipated within the vacuum chamber walls. Effects on beam stability of vibration and ground movements on a scale almost ten times larger than that of LEP, where even effects of nearby railroads and lunar tides could be observed, have also to be addressed [12, 91]. Finally the logistics of building, operating and maintaining a complex installation of that scale, no matter what particle is accelerated, would certainly require novel ideas and solutions.

2.2.3. Meson factories

General. Meson factories produce great quantities of meson–antimeson pairs by operating at c.m. energies corresponding to (or slightly above) resonances in the e^+e^- cross-section decaying dominantly into the desired particles: the ϕ resonance (1.02 GeV c.m.) for $K\bar{K}$ and the $\Upsilon(4S)$ resonance (10.58 GeV c.m.) for $B\bar{B}$. Four such e^+e^- colliders with design peak and average luminosities in excess of 0.1–10 $(\text{nb s})^{-1}$, one to two orders of magnitude higher than previously attained at comparable intermediate energies, have come into operation: the K-factory DAΦNE [22] and the B-factories PEPII, KEK-B [23] and CESR [24]. Their main parameters are listed in table 3.

All operate with a single IP, all except CESR-c, an upgrade of the existing single ring collider, have two separate rings and all, except PEP-II, have beams crossing at an angle.

All B-factories have exceeded peak luminosities of 1 $(\text{nb s})^{-1}$ and are being gradually upgraded towards $L > 10$ $(\text{nb s})^{-1}$. DAΦNE has reached 7.7×10^{-2} $(\text{nb s})^{-1}$, a record for its energy. All produce yearly average luminosities exceeding 60% of the peak [25].

Table 3. Meson factories (operational parameters [31]).

	KEKB		PEP-II			
Meson factories	LE	HE	LE	HE	DAΦNE (two rings)	CESR-c (one ring)
Max. beam energy, E (GeV)	3.5	8	3.1	9	0.51	5.3
c.m. energy (GeV)	10.6	10.6	10.6	10.6	1.02	10.6
Circumference, C (m)	3016	3016	2199	2199	97.69	768
RF frequency (MHz)	509	509	476	476	368	500
Number of bunches/beam, n_b	1224	1224	800	800	47	45
Bunch spacing, d (m)	2.4	2.4	2.5	2.5	2.08	4.8
Normalized crossing angle (full) (mrad)	1	1	0	0	0.38	0.18
Max. beam current/beam, I (A)	1.4	0.9	2	1.1	1	0.36
Beta functions: β_x^*, β_z^* (cm)	59, 0.6	61, 0.7	35, 0.9	50, 1.2	400, 4	96, 1.8
Damping decrement (10^{-4})	2.2	2.2	1.9	1.4	0.09	1.1
Max. achieved ξ_x, ξ_z (10^{-2})	8, 4.8	7.4, 4	6.2, 5.6	7, 2.9	2.5, 2.5	3, 7
Peak luminosity $(\text{nb s})^{-1}$	7.4	7.4	4.6	4.6	0.08	1.3
Bunch length (mm)	5.3	5.5	13	12	30	18
Peak RF voltage (MV)	9	15	5	14	0.2	6.7
Synchrotron radiated power, both beams (MW)	5.31	5.31	5.46	5.46	9.3E−02	0.86
Average power load/unit length (kW m^{-1})	0.7	1.0	0.7	1.8	0.5	1.1
Beam lifetime (h)			6	23.6	2	

KEK-B and PEP-II are asymmetric, meaning that their two rings have different energies adding up to the desired c.m. value. This because the physics goal—to measure differences in the decay modes of particle and antiparticle at threshold as a function of decay time—implies observing the two separate decay vertices and measuring their distances from the decay point. This is only possible if, the c.m. being in motion, the particle lifetimes are Lorentz-boosted so that origin and decay points of the pair become well separated. Detector requirements and machine considerations, such as having equal damping decrements in the two rings, argue for an energy ratio between 2 and 3. Luminosity is still given by equation (2.2.5) with $r \ll 1$,

$$L \cong \frac{c}{2r_0} \cdot \left(\frac{N_\mathrm{b}\gamma}{\beta_z^*} \right) \cdot \frac{\xi_z}{d}, \tag{2.2.13}$$

the design being such that the term in parentheses has the same value for both rings.

High peak luminosities are achieved by storing very large currents in many bunches, reducing the number of IPs and producing horizontal beam emittances larger than the lattice natural ones by inserting special wiggler magnets in the lattice [22], thus allowing N_b to increase for a same ξ_lim. Very low β_z^*s and correspondingly short bunch lengths are other necessary ingredients. High average luminosities are obtained through powerful full-energy injectors that allow frequent topping-up of the stored currents so as to effectively overcome the short luminosity lifetimes.

The main limitation on L has come from the so-called electron cloud effect which limits the maximum value of (N_b/d) in the e^+ ring. The effect, peculiar to high current multibunch e^+ and p machines, is caused by trapping, in and around the positive beam, of electrons originating mainly from photoemission by SR photons hitting the vacuum chamber walls. Electrons form an electron cloud surrounding the beam which can produce residual gas pressure bumps, tune spread, single and coupled bunch instabilities, malfunctioning of beam diagnostics equipment and, in SC machines, significant additional low temperature heat loads. Theoretical and experimental studies of the phenomenon have recently received much attention [26]. A much simplified description is as follows. SR photons absorbed on the vacuum chamber wall, mainly in the vicinity of the horizontal plane, produce primary photoelectrons that, in magnetic field free regions, are attracted towards the beam and accelerated in the electric field of passing bunches. The photoelectron yield per absorbed photon, $\bar{Y}$, depends on the chamber material, the photon energy and angle of incidence and can be as high as $\approx$10%. In a simple model assuming that quasi-stationary electrons produced at the walls of a chamber of radius R are accelerated in the field of a one-dimensional, uniformly charged bunch of N_b ultra-relativistic particles, the energy gained by such accelerated primary photoelectrons is $\Delta E \approx E = 2E_0 r_0^2 \cdot (N_\mathrm{b}/R)^2$ and can be as high as a few hundred eV. Photoelectrons produced inside bending magnets next to the ring midplane are harmlessly confined next to the wall by the vertical magnetic field but those produced by scattered photons that hit the chamber top and bottom walls can also spiral along magnetic field lines towards the beam.

Furthermore, some accelerated primary photoelectrons can traverse the chamber, hit the opposite wall and create low energy secondaries that can in turn be accelerated by the beam. The secondary electron yield depends on the primary energy and on the secondary emission coefficient δ. For ordinary chamber materials, electron energy in between $\approx$200 and 500 eV and normal incidence one has $\approx 2 \leqslant \delta \leqslant \approx 3$.

When the primary electron travel time across the chamber, τ, is less than or equal to the bunch separation $t = d/c$, a fraction α of secondaries is still drifting around when the next bunch comes along and can in turn be accelerated through the chamber starting a new cycle. If $\delta \cdot \alpha > 1$ and $d \leqslant R^2/(r_0 N_\mathrm{b})$, avalanche multipacting can develop independent of bunch length and the electron cloud can build up fast to its space charge limit. At the multipacting

threshold one has

$$E_{\rm thr} \cong 2E_0 \cdot \left(\frac{R}{d}\right)^2 \qquad \text{and} \qquad N_{\rm b\,thr} \cong \frac{R^2}{r_0 \cdot d}. \tag{2.2.14}$$

With typical factory numbers, $d \cong 1\,\text{m}$ and $R \cong 2\,\text{cm}$, one finds $N_{\rm b\,thr} \cong 10^{11}$ and $\Delta E_{\rm thr} \cong 0.4\,\text{KeV}$ [28].

The lens-like field of the cloud does introduce additional linear and non-linear terms in the beam equations of motion, causing coherent and incoherent tune shifts and resonance excitation. In addition, because the force felt by the beam particles traversing the cloud depends on the local cloud density and position, that in turn depends on the beam position, positive feedback mechanisms can develop producing single bunch and multibunch instabilities [26].

The e-cloud phenomenon is not yet fully understood and although synchrotron radiation (SR) itself does progressively clean the chamber surface (SR scrubbing) and special techniques—such as coating the chamber walls with low extraction coefficient materials, implementation of longitudinal solenoidal fields on straight sections—are applied, it does still limit the performance of B-factories.

High currents and many bunches require strict control of all other single and coupled bunch instabilities, which has prompted the development of novel fast bunch-to-bunch digital feedbacks now widely used in all multibunch accelerators [28].

Another major technical development, to stabilize the very high accelerated currents, has been that of 'single mode', high stored energy RF cavities both warm and cold, capable of standing extremely high beam loads and in which all dangerous HOMs are suppressed or strongly detuned. While the above requirements favour superconducting systems, because at factories the major part of the required power anyway goes to the beam and because SC technology had not progressed enough at the time when existing factories were designed, warm cavities have been generally used. Suitable SC cavities have been developed since, in particular at Cornell and KEK [29]. A DAΦNE warm cavity equipped with waveguide HOM absorbers to attenuate all undesired mode by one to two orders of magnitude [30] is shown in figure 5.

Next generation factories. The great success of factories in terms of physics and technology has triggered studies on second generation, super-B-factory (SBF) designs to produce luminosities up to $10^3\ (\text{nb s})^{-1}$. As an example, the kind of parameters tentatively considered [32] in order to achieve a 300-fold luminosity increase at PEP-II, and the corresponding factors to be gained over present performance, are listed in table 4.

A most striking feature of the design is the two orders of magnitude shorter lifetime, due to both luminosity burn-off and to the larger nominal ξ values, obtained by letting the beam tune footprint in collision come much closer to normally avoided resonance lines. With lifetimes of a few minutes continuous injection, by now a well-established practice [22, 33], is mandatory. Its feasibility in conjunction with all other design conditions remains however to be proven and its effects on the experimental detector physical integrity and backgrounds remain to be studied. A non-negligible positive return would be the raising of $\langle L \rangle$ to $\approx$95% of $\hat{L}$.

Other critical points, pinpointed in the paper as requiring extensive R&D, are the electron cloud effect, the design of IRs with very low equal β^*s for round rather than flat beams, beam stability at 10 times the present current, a low impedance vacuum chamber able to stand $\approx 16\,\text{KW m}^{-1}$ of SR.

Tau-meson [34] and neutrino factory projects are also being proposed. Neutrino factories based on muon storage rings promise to be a major importance breakthrough in accelerator

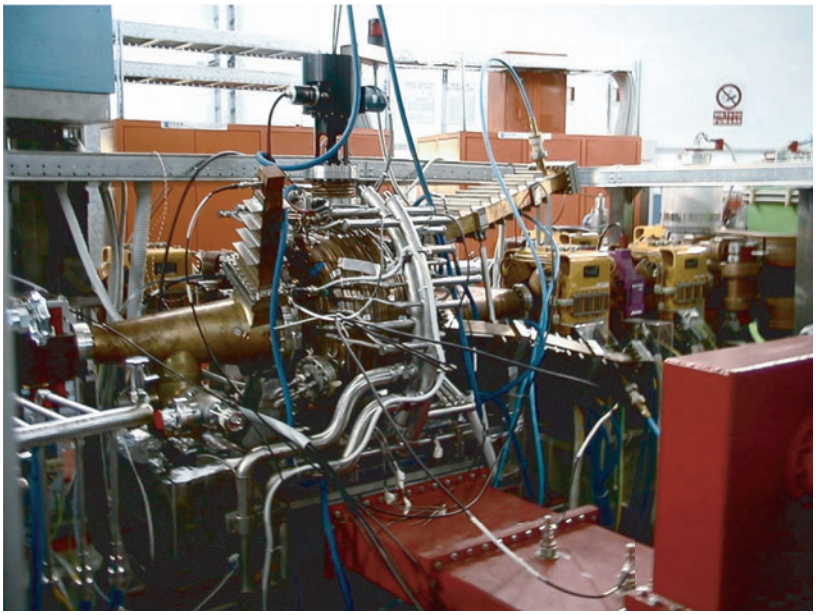

Figure 5. The DAΦNE cavity.

Table 4. Tentative parameters of a super-B factory. The ratio of SBF–PEP parameter values is also shown [32].

	SBF		SBF/PEP
	LE	HE	(approx.)
E (GeV)	3.1	9	1
Peak $L/10^{33}$ (cm^{-2} s^{-1})	1000	1000	300
I (A)	19	6.6	10
Number of bunches, n	3492	3492	2
β_x^*, β_z^* (cm)	0.3, 0.3	0.3, 0.3	1/15, 1/4
ξ_x, ξ_z	0.14	0.14	2
Peak RF voltage, V_{RE} (MV)	30	50	6, 3
SR total power, P_{SR} (MW)	38	38	10
Beam lifetime (h)	0.08	0.08	$<1/100$

technology. Being in a way a by-product of muon collider studies they are discussed in section 3.7.

2.3. Hadron colliders

2.3.1. General. Top energies of present generation $p\bar{p}$ colliders—the SppS at CERN and the upgraded TeVatron at FNAL [35]—and of future pp ones—LHC [36] and the VLHC being studied by a USA collaboration [15], whose main parameters are collected in table 6—are about two orders of magnitude higher than those of e-colliders of the same generation; their Lorentz factors are correspondingly about one order of magnitude lower. According to equation (2.2.9) the radiated power is thus four orders of magnitude lower than that of e-machines with comparable values of i and ρ_0. Additional many orders of magnitudes come in for heavy ions.

The energies of present and next generation hadron colliders are thus still essentially determined by, and proportional to the product of bending radius, ρ, and bending field, B_0 (equation (2.1.1)), the machine circumference being $C = F \cdot 2\pi \cdot \rho$ with F a filling factor accounting for the difference between the bending and the average radius. Because cost favours the shortest possible circumference, the achievable top energy depends heavily on the bending magnets field. The demand for HE has thus stimulated a worldwide R&D effort towards the development of superconducting main lattice elements which can reach high fields (HFs) while saving on operating costs. Progress in the technology of such components, aimed at higher and higher fields, appropriate field quality and affordable costs, has been very remarkable. Cooling plants, to remove tens of kW of power at liquid or even super fluid He temperatures from 1 km long strings of magnets, have also been developed in collaboration with industry [37].

Figure 6 shows how bending field, B_0, circumference, C, and L vary with the energy of major existing and proposed proton colliders: up to the LHC, C and B_0 both scale like $\approx\gamma^{1/2}$, thus equally sharing the burden of increasing energy, while L scales approximately like γ^2. Novel problems arise at higher energies that make next generation designs scale differently.

For reasons similar to those discussed in the e^+e^- case, high luminosity requires many bunches, circulating in separate vacuum pipes everywhere but in the IRs, and beams crossing at an angle.

Weakly radiating beams being practically undamped, their normalized emittance, that should ideally remain constant at its injection value, does in practice grow with time—because of resonance excitation, beam–beam induced tune spread, intrabeam scattering (IBS)—even when all other unwanted perturbations such as other space charge effects, RF noise, beam manipulations, non-linear forces, ground motion, vibration, etc, have been minimized or eliminated. The emittance blow up does eventually reduce $\hat{L}$ and beam lifetime.

Albeit still weak, radiation effects start to become noticeable in pp accelerators already at LHC energy and do affect both the vacuum environment design and the collider performance.

On the other hand, the radiation damping time τ_{rad}, even if much longer than the stored beam useful lifetime, does help keeping emittance diffusion in check.

Radiation affects the design of components, primarily that of the beam vacuum environment of the largest SC proton colliders equipped with cold bore magnets: disposing of heat deposited on the vacuum chamber by synchrotron radiation (SR), which makes up the

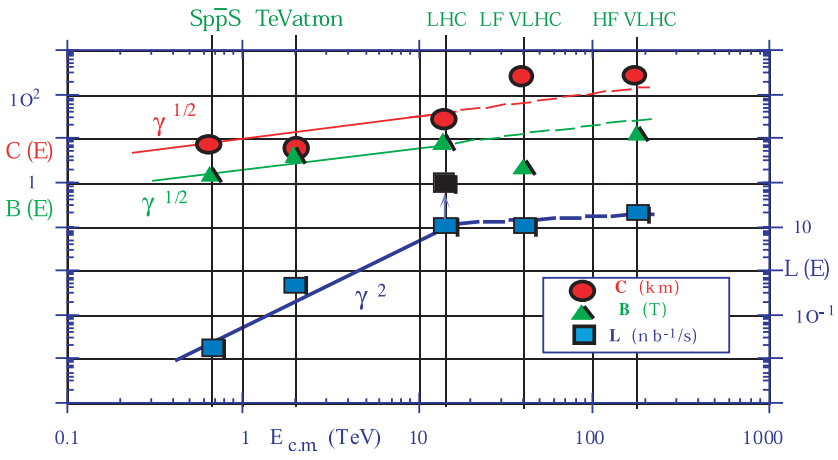

Figure 6. Proton colliders: circumference, bending field and L vs top energy.

largest fraction of the total cryoplant heat budget, is a major problem. The power deposited, at LHC, of the order of 0.2 W m^{-1}, is too large to be dealt with at super fluid He temperature. Perforated beam screens, kept at higher temperature, typically 50–70 K, are therefore inserted coaxially in the vacuum chamber to collect it. Maintaining mechanical stability of such screens over many km in the presence of quench-induced forces and temperature variations, ensuring good surface conditions and managing the additional impedance produced by the slotted walls, pose major design and manufacturing difficulties [38].

In general, the amount of energy stored in the beam, reaching into the GJ, concentrated in a beam with a fraction of a square mm cross-section, is so large that even the accidental loss of a minute fraction of it can produce catastrophic damage to the machine; complex, highly reliable protection systems have therefore to be implemented to timely detect any accidental particle loss and activate fast kickers to safely dump the whole beam in emergency or at the end of each run [39]. Another system of collimators and absorbers must protect experimental detectors and SC magnets, particularly IR ones, from stray particles and collision debris that at design luminosities can deposit large amounts of power into the apparatus. At LHC top energy and luminosity the interaction rate is $\approx 10^9$ events s^{-1}, corresponding to a debris power of $\approx$1 KW per beam, most of which ends up in the IRs [40].

2.3.2. p–p colliders

Technology. To meet both technical and cost challenges of superconducting bending and focusing lattice elements and of their cooling plants and accessories, intense R&D has been going on since several decades. Dipoles are usually the main cost driver but focusing quadrupoles, particularly very high gradient ones for IR final focusing, are technically equally challenging. It is crucial to design items that can be produced within strict tolerances in large industrial series at an affordable price. A large fraction of investment and operations costs of a SC system is in its end interfaces to the warm world; fabrication difficulties and cost of individual components, particularly dipoles, are also mainly in the ends, where coils bend around the bore. It is thus advantageous to make all elements as long as lattice design and magnet technology permit, a trend showing in figure 11.

A SC accelerator lattice therefore consists of long strings of cold elements—dipoles, quadrupoles, auxiliary multipoles, corrector elements—connected to each other inside an effectively single cryostating vessel, the length of which is determined by cooling plant requirements.

The over 1200, state-of-the-art, 8.3 T LHC dipoles and the LHC 25 T m^{-1} IR quadrupoles are at the limit of present technology. Figure 7 shows the structure of the dipole [41] whose main parameters are listed in table 5, and figure 8 shows an artist view of the accelerator layout in the tunnel. The cryostat enclosing all lattice magnetic elements, operating at 1.9 K, is continuous over each of eight 3.3 km long sectors. Every 53.5 m a connection box connects the magnet to the external LHe feed line.

Typical present generation accelerator magnets have saddle shaped coils that approximate the ideal current distribution, kept in place by stiff metal collars and surrounded by a laminated iron yoke enclosed in a steel vessel. As an example, cross-sections of the LHC dipole coil and of the whole assembled dipole ‘cold mass’, are shown in figures 9 and 10. The magnet double bore allows two separate rings to be accommodated in a single magnet.

The critical component limiting the top field value is the superconducting cable. So far accelerator magnets have used NbTi cable that needs to operate in the super fluid He regime, at 1.9 K, to reach its upper operational limit of $\approx$10 T. Persistent currents generated in the cable by field variations at injection have to be carefully studied and kept under control. Because of

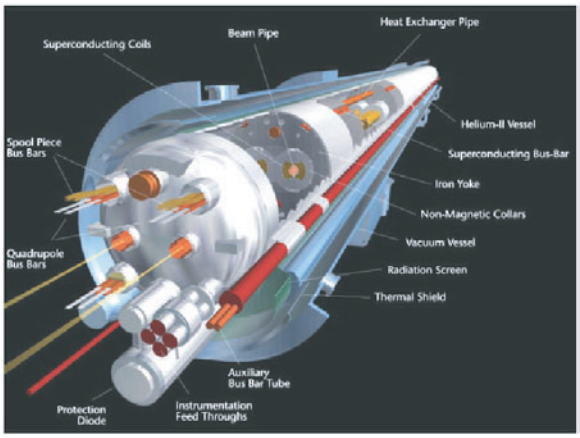

Figure 7. Cutout structure of the complete LHC dipole in its cryostat [41].

Table 5. Main parameters of the LHC dipole cryo-magnet.

Inject. field (0.45 TeV beam energy)	0.54	T
Nom. field (7 TeV beam energy)	8.33	T
Ultimate operational field	9	T
Nominal current	11 800	A
Stored energy at 7 TeV	7.1	MJ
Operating temperature	1.9	K
Magnetic length at 1.9 K	14.3	m
Nominal short sample field limit	9.65	T
Overall length with ancillaries	16.8	m
Bending radius	2812.36	m
Cold bore inner diameter	50	mm
Distance between apertures	194.52	mm
Cold mass diameter	570	mm
Mass of the assembly	∼27.5	ton

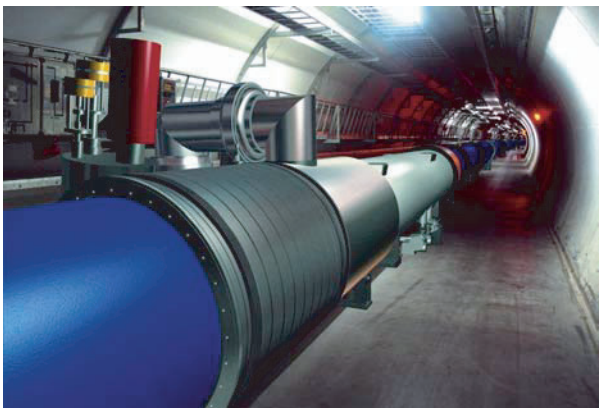

Figure 8. LHC tunnel: cryostat encloses all lattice magnetic elements. Part of a connection box shows at left. The He feed line is hidden behind the cryostat [41].

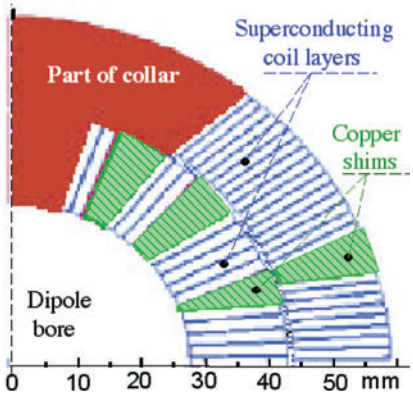

Figure 9. Schematic cross-section of $\frac{1}{4}$ of the LHC coil.

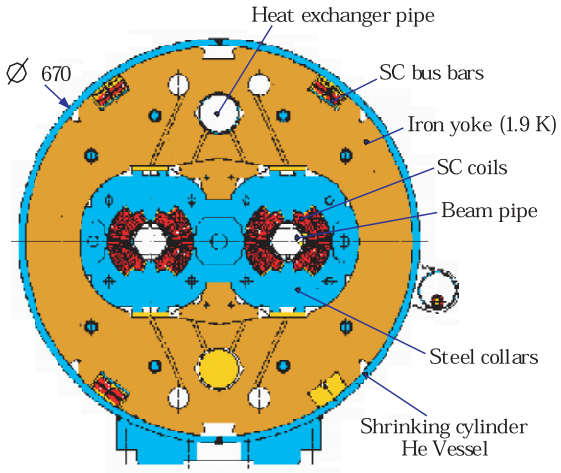

Figure 10. Cross-section of the LHC cold mass. The field has opposite polarity in the two bores; the iron yoke contributes ≈2 T to it [41].

the amount of stored energy, magnet quenches, whether self-induced or induced by accidental external heat inputs, can be destructive; appropriate quench protection systems have therefore to be implemented [35]. Finally, the coil has to stand high irradiation over many years of operation.

Major technical problems are also posed by the high stored energy $E_{\rm st} \propto B^2 a^2 l$, a being the bore radius and l the magnet length, and the consequent large forces acting on the coils, combined with the requirement of coil positioning to micrometre accuracy to achieve the desired field precision over the entire operating field range [43]. At top field forces tending to push the coil windings apart are measured in MN m^{-1}.

Figure 11 shows the evolution in time of field, bore diameter and length of major SC hadron collider dipoles with NbTi coils. Bores can be allowed to decrease as field increases because of beam emittance decreasing with energy; the stored energy per bore and per unit length, $\varepsilon_{\rm st}$, thus remains constant to within a factor of ≈2.

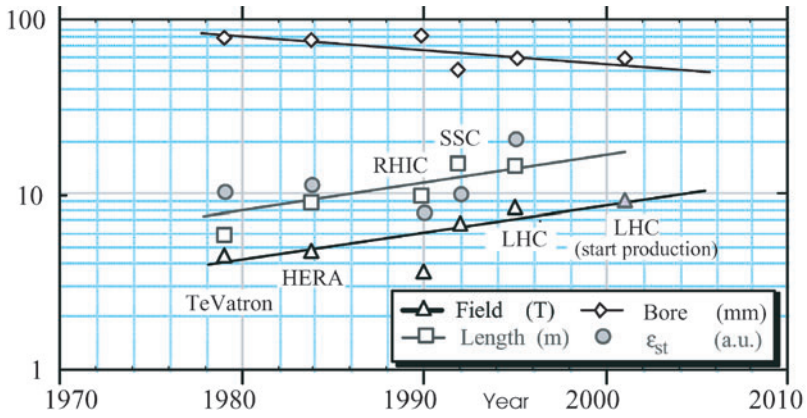

Figure 11. Field, bore radius, length and stored energy per bore of NbTi collider dipoles. The SSC magnet has been only prototyped. The LHC dipole is double-bored. All dates, except the LHC dipole production starting date, are those on which projects were started.

Performance. According to equation (2.2.5) luminosity is maximized when beams are round at the IP, which fits well with weakly radiating beams normally having equal radial and vertical emittances determined by the injected ones. One then has

$$L = \frac{c}{r_p} \cdot \xi \cdot \frac{N_b}{d} \cdot \frac{1}{\beta^*} \cdot \gamma_p \tag{2.3.1}$$

with r_p the proton classic radius, γ_p the Lorentz factor and $\beta_x^* = \beta_z^* = \beta^*$. According to scaling law (2.2.6), for undamped ($\delta \lessapprox 10^{-9}$) proton beams ξ_{lim} is in the 0.006–0.009 range. Extrapolation from experiment and simulation indicates that, for good luminosity and lifetime and low backgrounds, the total tune footprint should not overlap non-linear resonance lines of up to 12th order [44].

At c.m. energies in excess of ≈10 TeV, with expected 'discovery' threshold cross-sections of the order of the fb, peak luminosities $\geqslant 10\ (\text{nb s})^{-1}$ are required, when all accelerator and experimental efficiencies are taken into account, to collect a few thousand interesting events per year. The main cause of particle loss then becomes L itself. The particle loss rate (luminosity 'burn-off') is $\mathrm{d}N/\mathrm{d}t \cong -n_{IP} \cdot L \cdot \sigma_T$, with σ_T the particle total cross-section and n_{IP} the number of IPs. The resulting rigid beam luminosity half-lifetime $T_{1/2}$ and the corresponding integrated luminosity $L_{1/2}^{(int)}$ are given by

$$T_{1/2} \approx \frac{1}{2\sigma_T \cdot n_{IP}} \cdot \frac{n_b N_b}{L_0} \qquad \text{and} \qquad L_{1/2}^{(int)} = \bar{L} \cdot T_{1/2} \approx \frac{n_b N_b}{2\sqrt{2}\sigma_T \cdot n_{IP}} \tag{2.3.2}$$

with L_0 initial luminosity, $n_b N_b$ number of stored particles and n_{IP} number of IPs. The first equation shows that, as expected, because $L_0 \propto n_b N_b^2$, $T_{1/2}$ is proportional to $1/N_b$.

Magnetic optics and beam dynamics considerations define the minimum achievable value of β^*; at LHC it is ≈50 cm. It follows that for $L/E \geqslant 1\ (\text{nb s TeV})^{-1}$, (N_b/d) must be $\geqslant 5 \times 10^7\ \text{cm}^{-1}$. The total current, proportional to (N_b/d), is limited by total beam power, available mains power, cryogenic heat loads, (particle loss rate), electron cloud and parasitic long-range interaction effects. N_b itself can be constrained by single bunch instabilities, particularly at injection.

For given luminosity an upper limit on d is set by the number of collision events per bunch crossing, $n_{ev/Xing} = L \cdot \sigma_T \cdot (d/\beta c)$, constrained to stay below what the detectors can resolve.

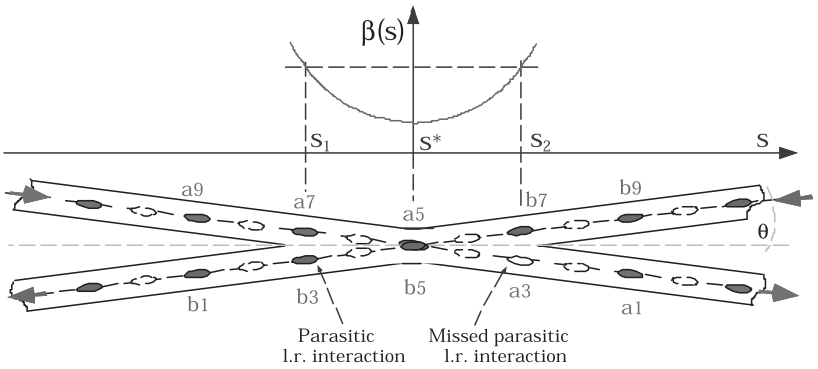

Figure 12. Schematic view of an IR straight section vacuum chamber with beams crossing at a small angle. Every other bucket is here empty. Because bunch $a3$ is missing bunch $b3$ misses the head-on collision. On top, the behaviour of the β function in the IR.

A lower limit $d_{\min} \leqslant d$ is instead set by parasitic long-range beam–beam interaction effects [45] when the IR stretch of common beam pipe through which both beams must pass is longer than one half the single beam bunch separation d as it usually the case; e.g. at LHC, $d \approx 8$ m while the common pipe is $\approx$125 m long. Even when beams cross at an angle 2θ, bunches passing each other transversely separated by $\delta_m \approx 2\theta \cdot md$ with m an integer still experience each other's long-range field (figure 12) undergoing unwanted 'parasitic collisions'. Particles with large oscillation amplitudes are the most affected by the resulting non-linear, largely coherent forces that produce additional tune shifts and orbit distortions and possibly coherent instabilities.

The problem is further complicated by the fact that—because gaps in the bunch train are needed to accommodate the rise and fall times of the various magnetic elements required, in the main ring and throughout its injector chain, for injection, extraction and beam dump—bunches are not uniformly distributed around the circumference. Bunches meeting with gaps, such as $b7$ in figure 12, miss out some parasitic collision or, when bunch distributions or IP positions are non-symmetric, even some head-on one.

Depending on the number and position of the missed collisions there are many different classes of such (in jargon) Pacman bunches, each with peculiar orbit distortion and tune shift. The overall tune spread grows considerably, as shown in the example of figure 13, and the orbit amplitude spread grows too. Larger aberrations are thus produced and coherent instabilities can develop that degrade the collider potential performance.

To minimize the effect the crossing angle must be large enough for the induced tune spread to remain much smaller than ξ_{lim}, but large enough for the beams to fit into the available aperture and for bunch overlap at the IP not to be significantly reduced. Special bunch train configurations must also be implemented and the tunes of the two rings must be carefully chosen [46].

An interesting possibility is offered by the fact that, because the β function s^2 dependence around the IP compensates that of the e.m. force, parasitic kicks felt by a bunch do not depend on where they occur. It is therefore in principle possible to compensate their effect by an external magnetic field generated by current carrying wires parallel to the beam, positioned at the two ends of the IR [48]. Simulations for the LHC show that the parasitic collision footprint would be greatly reduced and the technical implementation of the scheme is therefore being studied.

A different scheme to compensate both main and parasitic collision induced tune shifts is to be tested as part of the TeVatron $p\bar{p}$ upgrade programme, albeit at much lower energy and for fewer bunches. It would employ a bunched, low energy, high current electron beam, crossing the $\bar{p}$ one in a high β straight section, its bunches acting as compensating lenses on each $\bar{p}$ bunch individually. Simulations indicate that substantial footprint compression should be achieved [49].

Finally, electron cloud effects, in particular heat load from accelerated primary electrons hitting the cold vacuum chamber, have to be taken into account. As an example, from the simulation of the computed average heat load on the LHC beam screen as a function of N_b and δ, shown in figure 14, one sees that to reach the nominal $N_b = 1.1 \times 10^{11}$ value without

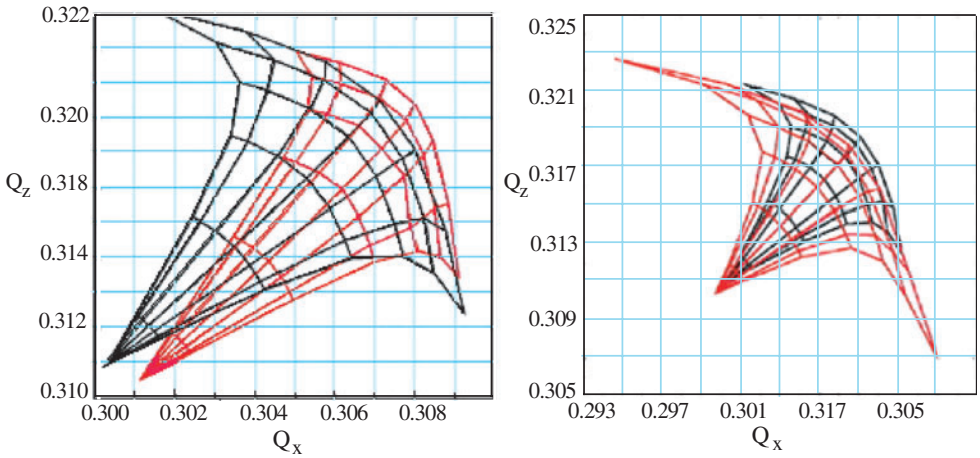

Figure 13. Examples of simulated tune spread in LHC: (*a*) 300 m rad (red) and 150 m rad (black) crossing angles. (*b*) Head-on collisions (black) and head-on plus parasitic ones (red) [47].

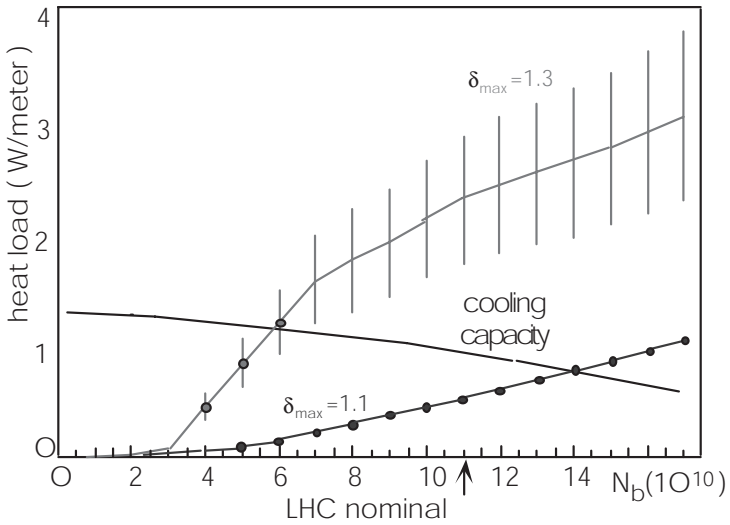

Figure 14. Heat load on the LHC vacuum chamber as a function of number of particles per bunch, N_b, and secondary emission coefficient δ [50].

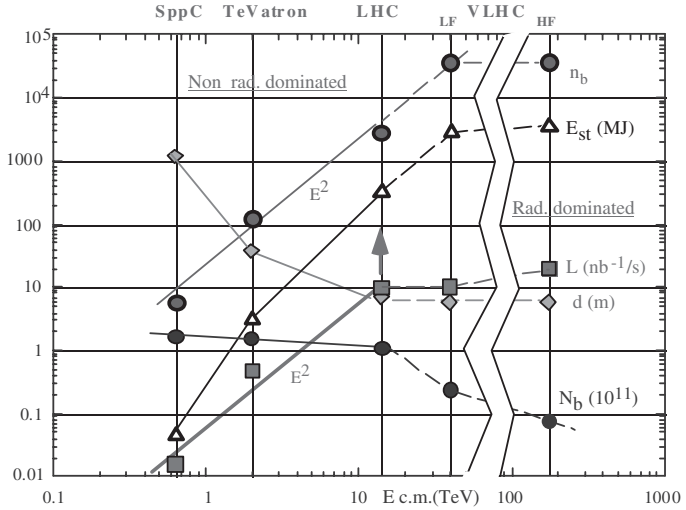

Figure 15. Proton collider parameters vs top energy. Current is the two beams average.

exceeding the installed cooling capacity, δ needs to be brought down to $\approx$1.1 [50]. Scrubbing of the chamber walls by the full energy circulating beam is expected to be sufficient to achieve the goal [51]. Simulations and experiments nevertheless continue, to better understand the phenomenon and the role of all parameters involved and to find ways, including improvements of vacuum chamber and beam screen designs and treatments, to reduce the effect [52].

Values of L, N_b, d and n_b of operating $p\bar{p}$ (SppS, TeVatron) and future pp colliders are plotted versus c.m. energy in figure 15. The SppS and TeVatron differ from the two higher energy ones in that their performance is mainly determined by the $\bar{p}$ beam achievable structure, intensity and emittance.

The graph shows that up to LHC energy, where d approaches $\approx d_\mathrm{min}$, L is kept scaling approximately like E^2, essentially by increasing n_b by more than two orders of magnitude at approximately constant N_b. It is seen that a further order of magnitude in energy over LHC introduces other constraints and consequently different scaling laws.

Future VLHCs. While most of the design criteria of LHC are based on the experience from previous machines further developments and novel schemes are being worked out for the after-LHC generation.

It is quite natural to consider a staged upgrade to LHC II [53] after some years of operation, when the machine performance will be fully understood and optimized, should the physics results justify it as hoped. The basic options being looked at are a ten-fold luminosity upgrade at present nominal energy and a two-fold energy upgrade when advances in magnet technology will allow reaching the corresponding top field. According to preliminary theoretical studies, the two options would be essentially equivalent in physics potential [2].

A tentative scheme for the first option envisages doubling both the circulating bunch current and the number of bunches and halving β^* by rebuilding the IR. The second option, expected to become technically viable not earlier than in the second half of the next decade, would instead imply raising the injection energy, which in itself would allow for lower injected emittance and therefore higher L, and installing an entirely new lattice with dipoles good for 15–17 T, cooling capacity included. Extensive interventions on most other auxiliary systems

would also most probably be required. Today's view of the status and perspectives of magnet R&D for LHC II is found in [54].

In the USA studies centre, as earlier mentioned, on the VLHC project. The latest version of this *pp* machine aims at an energy $\geqslant$100 TeV c.m., with $B_0 \gtrapprox 10$ T [21]. Its circumference is 233 km with an assumed filling factor close to 0.9 (as compared to LHCs 0.66).

The fact that achievable top bending fields tend to increase with time as better materials and better technologies are developed, has prompted the designers to devise a staged approach. In a first stage one would excavate the 233 km tunnel, compatible with the FNAL site, to house a 40 TeV c.m. collider equipped with inexpensive, low field (LF) magnets. In a second stage, when SC magnets with $B \geqslant 10$ T have become available, the first stage machine would be converted into an injector to a second, high field (HF), final energy collider housed in the same tunnel.

The 40 TeV c.m. first stage ring (LF VLHC) is equipped with 2 T hybrid design dipoles; the second stage, 180 TeV superconducting machine (HF VLHC), with the final $\geqslant$10 T dipoles.

For the LF VLHC a novel, cost effective, 2 T 'superferric' twin bore magnet is being studied. It uses a conventional warm iron yoke excited by a superconducting coil consisting of a 100 KA transmission line like conductor. A schematic drawing is shown in figure 16 [55]. The scheme proposes to combine the advantages of iron field shaping and of a simple SC coil located where the magnetic field is minimum. The bore diameter is only 20 mm. The protruding part of the vacuum chamber provides the required pumping conductance.

The HF dipole for the second stage, centring on cable wound with higher J_c materials such as Nb_3Sn, is being developed at LBL. Such cable does in principle allow reaching up to $\approx$15 T at 4.2 K. Because the material is brittle new coil winding techniques and new design concepts are being studied [55]. Coils are fabricated by the so-called 'wind and react' technique: the cable is manufactured from strands made of pairs of Nb and Sn filaments, wound in the desired coil shape and finally heated to high temperature until the filaments melt into the alloy.

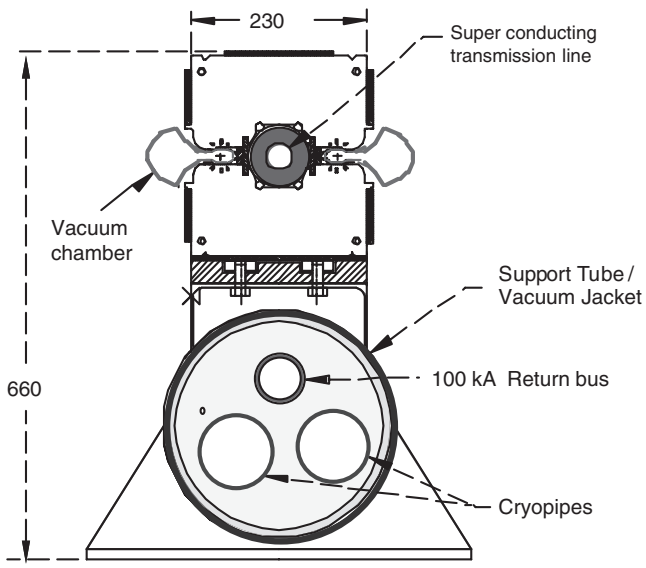

Figure 16. Conceptual design of a 'superferric' magnet for the LF VLHC [55].

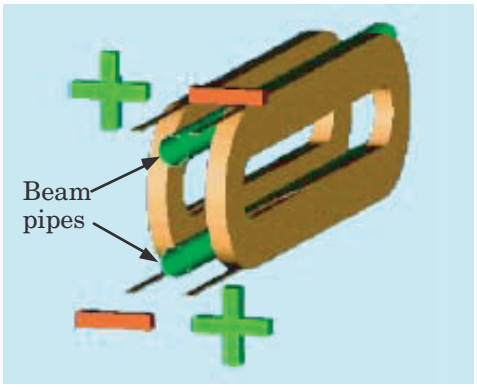

Figure 17. Common coil principle: ± signs indicate magnetic field polarity [56].

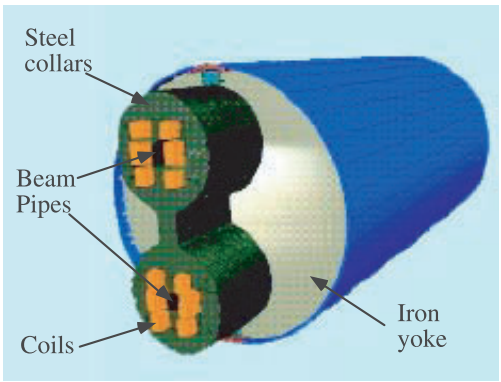

Figure 18. Common coil dipole assembly scheme [56].

A 'common coil' twin bore magnet geometry, using only two planar racetrack coils, simpler to react and wind and better suited to sustain the large magnetic force, is being tested. The principle and a schematic drawing of the magnet are illustrated in figures 17 and 18. A 1 m long prototype of this design has reached the record field of 14.7 T [55]. On the basis of past experience however, there is still a long way to go before tens of metres long magnets with the required field quality matching this performance can be built in industry.

HF VLHC would be the first example of a *pp* machine operating in the radiation dominated regime, when the radiation damping time τ_{rad} becomes short enough for equilibrium emittances to be reached in a time short compared to the luminosity lifetime. The beams then become flat after a few damping times, which makes the design of the IR optics technically easier. The minimum obtainable β^* value can be consequently smaller, allowing gaining back, at least in part, the factor of 2 ideally lost with respect to the round beam situation. β_{max} can also be lower so that particles encounter weaker non-linear field components and produce less SR, and fewer backgrounds in the detector.

Very HE and radiation dominated beam dynamics impose constraints different from those of lower energy machines.

First, because of hardware safety, cost and complexity considerations, the stored beam energy $E_{\mathrm{st}} = E \cdot n_{\mathrm{b}} N_{\mathrm{b}}$ must not exceed a threshold $E_{\mathrm{st}}^{(M)}$.

Second, in order to exploit the radiation-dominated regime, the lattice must be such as to satisfy $\tau_\beta \ll T_{1/2}$. From these two constraints one derives, using equations (2.3.2),

$$\bar{L} \cdot E < \left(\frac{1}{2n_{\mathrm{IP}} \cdot \sigma_{\mathrm{T}}}\right) \cdot \frac{1}{T_{1/2}} \cdot E_{\mathrm{st}}^{(M)}, \tag{2.3.3}$$

showing that for highest $\bar{L}$, $T_{1/2}$ and therefore τ_β should be short. Because $\tau_\beta \propto B^{-2}$, the need for the highest possible superconducting dipole field is again obvious.

Third, the cryogenic plant must handle the power $P_{\mathrm{rad}} = 2 \cdot n_{\mathrm{b}} N_{\mathrm{b}} \cdot E/\tau_\beta$ deposited by radiation in the cold environment with sufficient reserve to allow for static losses, other possible heat sources such as electron cloud effects and plant reliability. The installed cryogenic capacity P_{cryo}, defined by practical technology and cost considerations, imposes the additional design constraint $P_{\mathrm{rad}} < P_{\mathrm{cryo}}$. From equation (2.3.3) one then derives

$$\bar{L} \cdot E < \left(\frac{1}{4n_{\mathrm{IP}} \cdot \sigma_{\mathrm{T}}}\right) \cdot \frac{\tau_\beta}{T_{1/2}} \cdot P_{\mathrm{cryo}}. \tag{2.3.4}$$

For given energy and provided the needed values of ξ, emittance and beta functions at the IP are obtained, $\bar{L}$ is thus ultimately determined by either cooling capacity or stored energy.

Major difficulties are expected to arise in such future designs from e-cloud effects, stability of the several times higher bunch peak current, machine protection, number of events per crossing and backgrounds in the detector.

Rather recently an alternative scheme has been proposed to achieve very high luminosity while alleviating some of the above problems through the use of a different acceleration technique [57]. The basic observation is that single bunch instabilities, the beam–beam limit, electron cloud effects and, to some extent, detector limitations arise from the fact that, due to presently used high frequency accelerating resonators, the accelerated current is necessarily bunched in many short, dense bunches that occupy a very small fraction of the machine circumference. As an example, at LHC the fraction, f_{occ}, is only $\approx$2%. On the other hand it can be shown that, for same current density and same beam–beam limit, were the current distributed in much longer bunches so that $f_{\mathrm{occ}} \approx 1$, luminosity could be higher approximately in the ratio of the occupation factors [58]. This of course at the expense of increasing the circulating current by the same factor. The novelty is in using a system of non-resonating pulsed induction gaps to accelerate the beam in the main rings and keep it bunched, when coasting, in microsecond long, longitudinally rectangular 'super bunches'. Papers proposing to apply the technique to LHC II and to the VLHC, to reach peak luminosities in the 100 $(\mathrm{nb\,s})^{-1}$ range have been presented [59]. It is recognized that parasitic collision effects, vacuum chamber and beam screen design, cooling capacity and stored energy problems for an order of magnitude larger stored currents remain to be studied in detail.

Concerning e–p colliders, studies have been made of a HERA-TESLA, linear against circular machine to be part of the TESLA programme [6] and of various e–p options consisting in adding an electron ring in the tunnel of a VLHC (see table 6).

An example is the 80 GeV/3 TeV, 1 TeV cm, 0.3 $(\mathrm{pb\,s})^{-1}$ luminosity e–p collider designed to fit in a 340 km long 'VLHC' tunnel, the proton ring being similar to the LF VLHC ring [60]. e–p options in the LHC tunnel have also been envisaged.

2.3.3. Heavy ion colliders. The first dedicated, superconducting ultra-relativistic heavy ion collider, RHIC [61] has successfully come into operation in the year 2000 [62]. With its two completely separate rings, capable of operating at different bending fields, it can collide different ion species, from polarized protons to Au_{197}^{79}, with same Lorentz factor γ. Its

Table 6. Parameters of the highest energy future pp colliders.

	SpS	TeV33	LHC	LF VLHC	HF VLHC
c.m. energy E (TeV)	0.64	2	14	40	175
Lorentz factor	341	1066	7460	21 315	93 254
Dipole field B/store (T)	1.4	4.34	8.33	2	9.765
Circumference (km)	6.90	6.28	26.66	233.04	233.04
Number of bunches	6	121	2835	37 152	37 152
Bunch population* ($/10^{11}$)	1.70	2.7	1.1	0.260	0.075
Bunch spacing (m)	1150.0	39.6	7.5	5.6	5.6
Stored energy per beam (MJ)	0.05	5.2	352	692	1073
Beta functions at IP, $\beta^*_{x/z}$ (m)	0.6/0.15	0.35	0.5	0.3	3.7/0.37
Invariant radial emittance e_{nx} (μm)	*1*	*0.3*	3.75	1.5	0.04/0.004
Rms energy spread s_y ($/10^{-4}$)			1.11	0.6	0.5
Number of IPs	3	2	2	2	2
Crossing angle at IP (μ rad)	0	136	300	153	10
Peak luminosity, L (nbarn s)$^{-1}$	0.016	0.16	10	10	20
Beam-beam parameter, $\xi_{x,z}$	0.007	0.01	0.0034	0.002	0.008
Number of interactions/crossing	2.7	1.3	19	20	49
Debris power per IP (kW)	—	—	*3*	3	73
Dipole heat load $\eth\, \mathrm{d}P/\mathrm{d}s$ (W m^{-1})	10	3	0.2	0.09	7.9
Damping decrement	5.58E−14	2.53E−12	2.40E−10	4.73E−10	4.36E−08
R (Lumi half-life/damping time)	1.72E−04	4.11E−02	2.77E−02	0.10	1.30

Table 7. RHIC and LHC performance in the heavy ion collision mode.

	RHIC (Au^{79}_{197})		LHC
Parameter	Nom	Upgrade	Pb^{82}_{208}
Single charge beam energy (GeV)	250	250	7000
Total c.m. energy (TeV)	41	41	1148
Top c.m. energy per nucleon (GeV A^{-1})	201	201	5519
Circumference (km)	3.83	3.83	26.66
Number of IPs	6	6	2
Filling time (m)	1.4	1.4	10
Ions per bunch (10^{10})	0.1	0.1	0.01
Number of bunches per ring	60	120	608
Beam stored energy (kJ)	200	389.6	5584
Transverse emittance (initial) (π μm)	15	15	1.5
β^*, ξ (m)	2, 0.0016	1, 0.004	0.5, —
Luminosity (mb^{-1})	0.8–3	8	0.8–2
Luminosity lifetime (h)	10	10	10
Number of dipoles	396	396	1232
Maximum arc dipole field (T)	3.45	3.45	8.34
Arc dipole length, effective (m)	9.45	9.45	13
Number quadrupoles	492	492	400
Maximum arc quad gradient (T m^{-1})	71.2	71.2	233

parameters are compared to those of the forthcoming LHC, also capable of colliding ion beams up to Pb^{82}_{208} [63], in table 7.

The ion beam energy being Z_i times the single-charge energy, the total c.m. energy $2E_i$ in fully stripped heavy ion collisions is extremely large. For nucleon–nucleon collisions the relevant parameter is rather the c.m. energy per nucleon $2E_i/A$, with A the ion atomic weight.

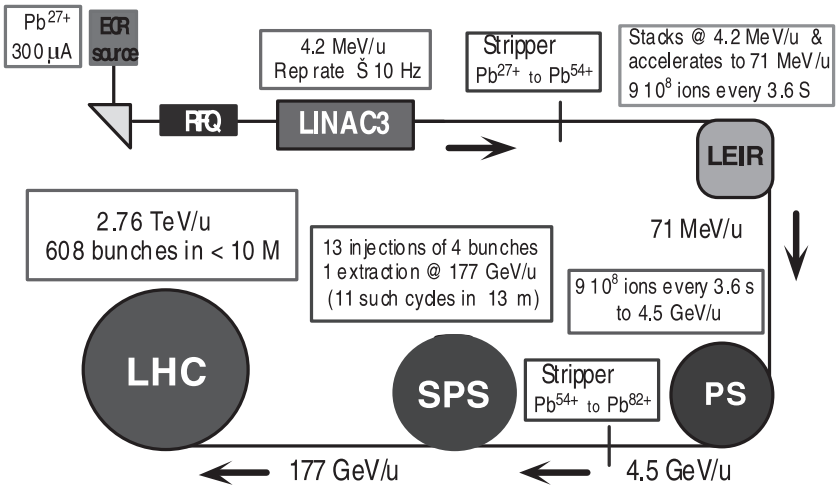

Figure 19. The LHC heavy ion production and injection chain [64].

Producing intense ion beams for injection into the final collider storage rings requires state-of-the-art sources and complex accelerator systems, the ions having to go through several stages of acceleration and stripping. Because of the large electron capture and ionization cross-sections, residual gas pressure of less than a few 10^{-10} Torr must be maintained throughout. Figure 19 shows a block diagram of the foreseen LHC ion production and injection chain. It comprises the LEIR storage ring—an upgrade of LEAR, formerly used to cool $\bar{p}$ for the SPS—dedicated to electron-cooling the ion beam to reduce its emittance to LHC injection requirements [64]. RHICs system is only slightly simpler [61].

The nominal luminosity of both machines, scaling roughly like A^{-2}, is of order 1 (mb s)$^{-1}$ for the heaviest ions. The value, much lower than for proton collisions, results in comparable reaction rates because of the much higher cross-sections. The kind of challenges the detectors must face because of the complexity of the ion–ion events is evidenced by figure 20, showing one of the first full energy Au–Au collisions seen at RHIC by the STAR apparatus [65].

Rather than by the beam–beam tune shift, nominal luminosity and store time are limited by collision rates and IBS.

The dominant cross-sections in collision are electromagnetic rather than nuclear: they change the ion Z/A ratio thus causing it to be lost. The largest one is for e^+e^- production by an ion in the e.m. field of the other beam. The ion energy loss is negligible but the abundant electron production results in a high probability of the e^- of a pair being captured immediately into an ion K-shell. The next frequent reaction is e.m. field induced break-up of the ion into smaller fragments (Coulomb dissociation). At RHIC, under nominal luminosity conditions and with two active IPs, the particle burn-off due to collisions, proportional to L, leads to a beam current lifetime $\tau_I \approx 60$ h.

The effect of IBS is much more severe. It causes particle diffusion in transverse and longitudinal phase space, leading to particle losses and transverse emittance blow-up that progressively reduce luminosity. It depends on the bunch particle density and, because it scales like $(Z^2/A)^2 \approx Z^2/4$, the diffusion rate of high Z ion beams is high even at the relatively low specified values of N_b. In transverse phase space, the emittance is blown up by factors of 2–3 during a store, while diffusion in longitudinal phase space causes the beam to gradually fill the RF buckets until particles start spilling out and be lost. Notwithstanding

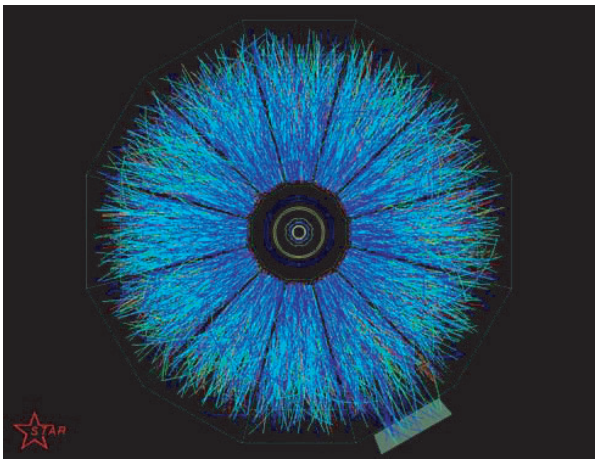

Figure 20. Tracks from an Au–Au event collected by the STAR detector at RHIC. The beam goes through the centre and one is looking into the apparatus in the beam direction. Dark radial lines are part of the detector supporting structure [65].

RHICs strong focusing lattice and a comparatively large chamber aperture, IBS induced losses produce a lifetime of ≈20 h only [66]. The combination of collision and IBS losses thus tends to make luminosity fall off rather rapidly. An efficient system of collimators is needed to intercept the lost particles and keep backgrounds in the experimental detectors acceptable.

To compensate IBS diffusion it has been proposed by several authors to continuously electron-cool hadron beams directly at the collider operating energy [67, 68]. The scheme asks for a high intensity, bunched, cold electron beam, injected at one end of a main ring straight section (SS) in which a high solenoidal field is maintained, and extracted at the other end. Electron bunches would travel superimposed on the ion ones, at the same speed and in the same direction.

To upgrade RHIC's performance the installation of two identical cooling systems, one for each of the main rings, is being considered. Each electron beam would be produced by a SC Linac, passed through a main ring straight section, extracted and fed back into the Linac so as to recover most of its energy. On the collider straight sections one would need to install 1 T, 40 m long solenoids with specified field precision of 10^{-5}.

Cooling would reduce the transverse emittance to the point where the beam–beam tune shift, ξ, again becomes the limiting factor. The beam size could also be adjusted as current decreases so as to keep $\xi = \xi_{\rm lim}$ over a large fraction of the store time. This, more bunches and a lower β^* are expected to upgrade $\hat{L}$ by a factor >10 (table 7) while keeping $\langle L \rangle \approx \hat{L}$.

Direct cooling of a HE beam has so far never been implemented and, particularly when dealing with high Z particles, the scheme is faced with a number of physics and technological challenges such as electron capture by the fully stripped ions to be cooled, electron beam steering, injection and extraction, energy recovery.

3. Very HE lepton accelerators

3.1. e^+e^- Linear colliders

3.1.1. General description. The LC concept originated as early as in the 1960s [19] but the first proposal of application to 'beyond LEP' energy machines, to circumvent the radiation

problem, dates from 1976 [20]. Linear accelerators (Linacs), on which LCs are based, are single pass, radiation-free, constant current generators that continuously accelerate a stream of bunches from source to final energy. Either e^+e^- or e^-e^- collisions can be produced since either charge can be indifferently accelerated. The possibility of accelerating polarized particles and of producing $\gamma\gamma$ and γe reactions, that can give access to different new final states with cross-sections that may be much higher than for e^+e^-, opens up in addition a rich, complementary physics programme.

The first (quasi) linear e^+e^- collider, contemporary to LEP, was the 90 GeV c.m., 5×10^{-3} $(\text{nb s})^{-1}$ SLAC LC (SLC) in Stanford [9]; it did lay the technological foundations of such machines. Next generation designs, under study since a number of years in Europe, in the US and in Japan, aim at energies in the TeV range, with ≈ 10 $(\text{nb s})^{-1}$ luminosities.

The LC main performance and cost driver is the accelerating structure itself, for which both superconducting and warm solutions are being proposed in competition with each other. Letting i be the average accelerated current and $G(s)$ the accelerating electric field[2], the power to be supplied to the beam by the accelerating system is

$$P_\text{b} = i \int_0^l G(s)\,\text{d}s = i \cdot \left(\frac{E}{q}\right) \qquad i = qN_\text{b}f, \tag{3.1.1}$$

l being the accelerator length and i the average current of a bunch train with bunch repetition frequency f and bunch population N_b. From equations (1.1.1) and (3.1.1) follows the important relation between beam power, luminosity and beam energy

$$P_\text{b} = \frac{S^*}{N_\text{b}} L \cdot E, \tag{3.1.2}$$

showing that, for given S^* and therefore for given beam emittance, high luminosity means high beam power. The overall power consumption of the installation, $P_\text{AC} = P_\text{b}/\eta_\text{AC}$, depends on the overall wall plug to beam power efficiency, η_AC, and must be kept within affordable and socially acceptable limits; it is usually therefore an input parameter. It follows that, for luminosity to keep pace with energy and for cost per unit energy to compete with that of present circular machines, power efficient acceleration schemes and high gradients to minimize the accelerator length are essential ingredients. They are however not the only ones. In fact, for same energy and beam power, the comparison of equation (3.1.1) with $P_\text{b} = i \cdot (U_0/q)$ holding for a circular machine shows that the LC average current is lower at least in the ratio (U_0/E). Furthermore, at cost-optimized gradient values, the maximum tolerable average dissipated power in the accelerating structure, whether cold or warm, imposes pulsed RF operation, with duty factors defined as $F_\text{D} = f_\text{rep} \cdot \tau_\text{p}$, with f_rep and τ_p the RF pulse repetition frequency and duration, respectively. Present F_D design values are in the $\approx 10^{-2}$–10^{-4} range, depending on the accelerator energy and technology, so that the average bunch repetition frequency is also much reduced with respect to that of a circular machine. Finally, given the minimum tolerable bunch separation, the collision frequency $f_\text{coll} = n_\text{b} \cdot f_\text{rep}$ is two to three orders of magnitude smaller than in a circular collider.

A further important difference with respect to circular machines however exists that allows compensating for the lower average current: because each bunch undergoes a single collision, beams can be focused down to much smaller size and higher charge density before beam–beam related limits on luminosity arise. Higher luminosity for given current can thus be obtained by squeezing bunches down so much that they emerge from collision completely 'disrupted'

[2] The 'voltage gradient' is for short called 'gradient'.

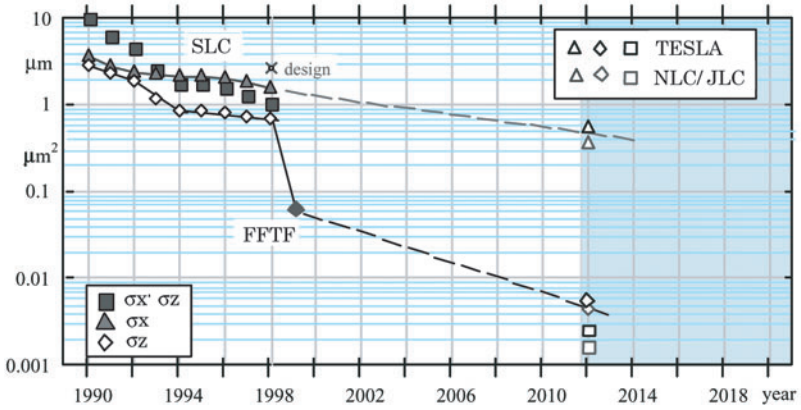

Figure 21. Beam dimensions in LCs. The point marked FFTB has been measured at the SLAC final focus test beam facility [69]. The cross-hatched area indicates that the new TeV colliders are not expected to come into operation before 2015.

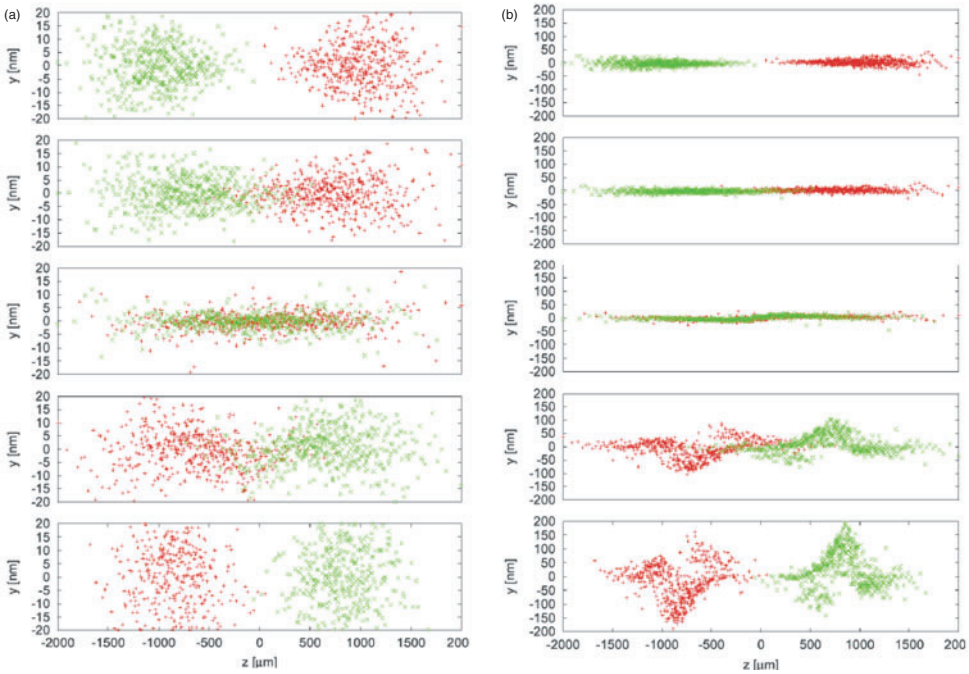

Figure 22. Pinch simulations under two different sets of initial conditions [70]. Ordinates are vertical and abscissae longitudinal particle positions, respectively, time runs downwards. The initial 'hourglass' bunch shapes reflect the β function behaviour.

(see figure 22). As shown in figure 21, beam transverse sizes a few orders of magnitude smaller than those of circular colliders and of the SLC are needed together with β^* values down to fractions of a few μm and, therefore, with comparably short bunches. Small enough transverse and longitudinal beam emittances and strong enough final focusing are of course prerequisites.

3.1.2. Luminosity and beam dynamics. Using equation (3.1.1), luminosity can be written for Gaussian bunches as:

$$L = \frac{n_b N_b^2 f_{rep}}{(4\pi\sigma_x^*\sigma_z^*)/H_D} = \frac{\eta_{AC} P_{AC}}{E} \cdot \frac{N_b}{4\pi\sigma_x^*\sigma_z^*} \cdot H_D, \tag{3.1.3}$$

H_D being a factor added to account for the cross-section pinch caused by the very strong e.m. fields inside the bunch that focus the colliding bunches further down. A measure of the e.m. field strength in the bunch rest frame, in units of the Schwinger critical field B_c, is the adimensional parameter Y given by

$$Y = \gamma \frac{|\vec{E}| + |\vec{B}|}{B_c} \approx \frac{5r_0^2}{6\alpha} \cdot \frac{N_b}{\sigma_y\sigma_x(1+r)} \cdot \gamma \qquad \text{with } B_c = \frac{m^2c^3}{e\hbar} \approx 4.4 \times 10^9\,\text{T}. \tag{3.1.4}$$

The pinch effect clearly shows in the simulation of figure 22(*a*). Because beams emerge disrupted, H_D is usually called, somewhat misleadingly, disruption enhancement factor.

The beam–beam interaction is in fact best characterized by the disruption factor defined in section 2.2, now much larger than one, and given, in terms of beam parameters, by

$$D_{x,z} = \frac{2}{\gamma} \cdot \frac{r_0 N_b}{\sigma_{x,z}(\sigma_x + \sigma_z)} \cdot \sigma_y. \tag{3.1.5}$$

showing that when $D \gg 1$ the beam–beam equivalent thin lens focal length is much shorter than the bunch length (see equation (2.2.4)). Disrupted bunches emerge from the IP with a large angular spread, and have to be carefully steered away from the detector to minimize backgrounds. The beam crossing angles at the IP should therefore preferably be large ($\theta_n > 1$). A clever way of allowing for large crossing angles without affecting luminosity is to tilt bunches in the crossing angle plane in such a way that they pass through each other head-on at the IP. This is done by an arrangement of high frequency transverse electric fields upstream from the IP.

A schematic diagram of the so-called 'crab crossing' scheme is shown in figure 23. The scheme is in practice rather complicated and this is why the TESLA LC design study, exploiting its large bunch separation, goes for head-on collisions instead, the separation being made downstream by a system of pulsed elements. The detailed implementation of the solution is still under study.

Particles crossing the strong e.m. field of the high-density bunch they collide with radiate, a phenomenon called beamstrahlung. In the classical limit $Y \ll 1$ and the radiated power is $P_{rad} \propto (\gamma B^2) \propto Y^2$. In the extreme quantum regime, when $Y \gg 1$, $P_{rad} \propto Y^{2/3}$ [71]. Radiated photons, the harder the higher is the field strength parameter Y, not only increase the collision energy spread ΔE but also create e^+e^- pairs and, colliding with beamstrahlung photons from the opposite bunch, e^+e^- mini jets that become a main source of backgrounds in the detector. It can be shown that when $Y \gg 1$ the average beamstrahlung induced energy spread is

$$\delta_B \underset{Y\gg1}{\approx} \left(\frac{\alpha^2\sigma_y}{1.7r_0}\right) \cdot \frac{Y^{2/3}}{\gamma}. \tag{3.1.6}$$

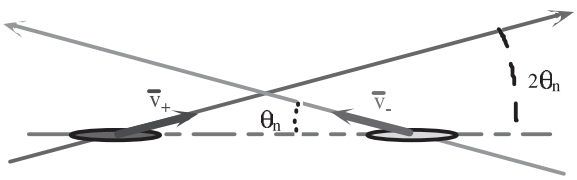

Figure 23. Crab crossing scheme.

The bunch behaviour during crossing is sufficiently complicated for the scaling laws $H_D(D)$ plotted in figure 24, accurate to ≈10%, having to be derived from simulation. For flat beams the parameter $A = \sigma_z/\beta^*_{x,y} \approx 1$ is a measure of the effect on the interaction of the inherent divergence of the incoming bunches.

Round beams appear much favoured but, in practice, several other considerations favour flat beams instead. In the first place for a round beam D_z cannot be larger than ≈5, or any initial offset $\delta_{x,z}/\sigma_{x,z}$ in the relative position of the crossing beams at the IP will trigger a kink-like instability, with bunches oscillating coherently in each other's field, thus drastically lowering luminosity. The effect shows in figure 22(*b*). For flat beams D_z must still be kept below the limit but D_x can be made much larger. Flat beams, that make the design of the IR optics and chromaticity correction easier, also allow for larger crossing angles in the horizontal plane for same luminosity

Last, because $r \ll 1$, Y and hence δ_B become independent from σ^*_z. To maximize luminosity the latter can thus be reduced, without affecting δ_B, to its ultimate limit determined by the the minimum achievable tolerances on the trajectory vertical position, all the way through to the IP.

Finally, N_b is obtained from the best compromise between maximum beam power P_b, minimum energy spread and minimum wake field amplitudes.

As for $\gamma\gamma$ collisions, the scheme is shown in figure 25. Compton backscattered photons are generated by focusing high power lasers on the electron beams at some distance upstream

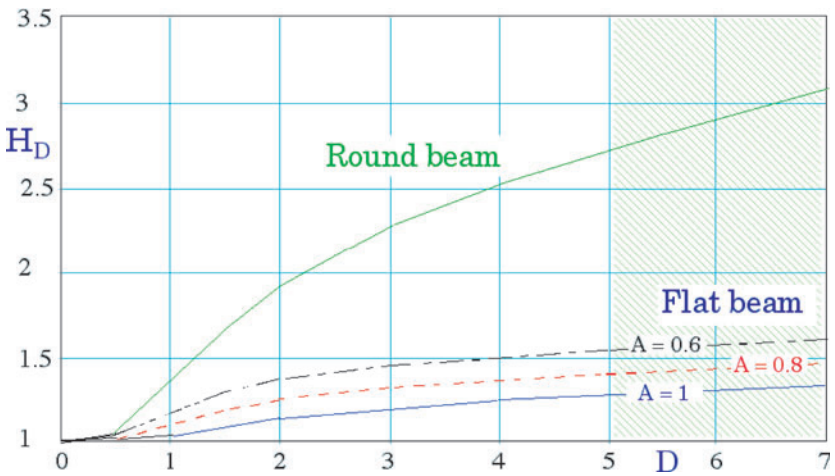

Figure 24. Disruption enhancement H_D vs disruption factor D as a function of parameter A.

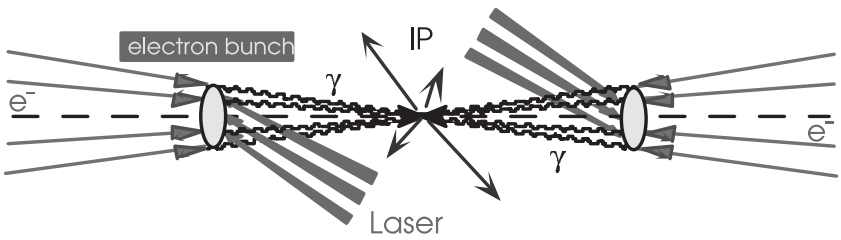

Figure 25. Electron conversion and $\gamma\gamma$ collision scheme.

from the IP. The two scattered photon beams, whose top energies are close to those of the parent electrons and emitted within $\approx 1/\gamma$ around the e beam direction, collide with each other at the IP while the spent electrons are swept away in a magnetic field. The highest scattered photon energy $h\nu_{\mathrm{ph}_M}$ is given by

$$\gamma_{\mathrm{ph}_M} \equiv \frac{h\nu_M}{E_{\mathrm{e0}}} = \frac{x}{x+1} \cdot \gamma \qquad \text{with } x \equiv 4\gamma \cdot \frac{h\nu_{\mathrm{las}}}{E_{\mathrm{e0}}} \cdot \cos^2\alpha_0 = 4\gamma\gamma_{\mathrm{las}}\cos^2\alpha_0, \tag{3.1.7}$$

E_{e0} being the electron rest energy, $h\nu_{\mathrm{las}}$ the laser photon energy and $2\alpha_0$ the angle between the electron and the laser photon velocities. As an example, at $E = 250\,\mathrm{GeV}$, $\alpha_0 \ll 1$ and $h\nu_{\mathrm{las}} = 1.17\,\mathrm{eV}$ ($\lambda = 1.06\,\mu\mathrm{m}$) one finds $x = 4.5$ and $\gamma_{\mathrm{ph}_M} = 0.82$.

Because the process is unaffected by beamstrahlung and the photon beam spot size at the IP is almost the same as would be that of the electron beam, luminosity can be increased by focusing down the electron to the ultimate limit allowed by emittance, optics aberrations and tolerances. The conversion efficiency of electrons into the highest energy photon fraction being ≈ 0.3 [72], the $\gamma\gamma$ luminosity becomes $L_{\gamma\gamma} \approx 0.3^2 L_{ee} \approx 0.1 L_{ee}$, with L_{ee} the 'virtual' e^+e^- luminosity corresponding to the limit e^+e^- IP spot size.

A major problem of the scheme is the need for high repetition rate lasers with terawatt peak power in ps long pulses, average power in the 50–100 KW range and sub-ps jitter.

3.1.3. Electron and positron sources. For high luminosity high peak and average current, and low emittance or, in other words, high brightness (defined as $B_n \propto \hat{\imath}/\varepsilon_n^2$), short bunch length electron and positron beams are needed. The physics and technology of generating and transporting such beams are in fact crucial R&D items not only for LCs but for other applications such as short wavelength free electron lasers (FELs) as well. One important advantage of a linear accelerator is that its initial normalized (invariant) beam emittance, ε_n, is determined only by the particle source. Provided ε_n is preserved throughout acceleration, the geometric beam emittance, $\varepsilon = \varepsilon_n/\gamma$, can thus in principle be made very small, the smaller the higher the energy.

Given the highest energy colliders performance specifications, the state-of-the-art brightness of e^- sources is still too low, at typical injection energies, for electrons to be directly fed into a collider Linac, particularly when considering that injected emittances are normally further diluted during acceleration. The brightness of e^+ sources is much too low. The source beam emittances must therefore be radiation damped by keeping the e beams coasting in intermediate damping rings with low enough equilibrium emittance values for a sufficient number of damping times. Because the damping ring must accept the full complement of N_{b} bunches forming a Linac pulse, injected and extracted on a bunch to bunch basis, the bunch train is normally first compressed by reducing the bunch separation to the minimum allowed by the rise and fall times of the injection and extraction kicker magnets and then re-expanded at extraction. A side benefit of using damping rings is that they naturally produce flat beams with $r \ll 1$.

Low emittance e^- sources of unpolarized electrons are based on RF gun devices in which ($\approx$round) electron beams are produced by a laser illuminated photocathode placed inside a high field (HF), RF accelerating cavity. The laser allows extracting high charge densities in short pulses, its pulse shape and pattern directly generating the desired electron bunch shape and bunch train configuration. One normally uses CsTe photocathodes with quantum efficiencies (QE) of $\approx 10\%$ in the UV region and months long life times under practical, $\approx 10^{-9}$ Torr operating pressures [73].

The HF ($\approx$50–100 MV m^{-1}) cavity provides very fast acceleration, thereby minimizing emittance blow-up due to defocusing space charge forces scaling like $1/\gamma^2$. The space charge

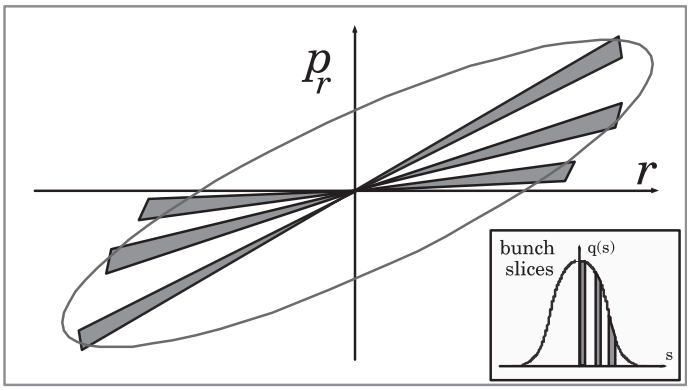

Figure 26. Fan-like slice emittance produced by space charge forces (schematic). The corresponding effective geometric emittance ellipse is also shown.

force in fact acts, to first order, as a defocusing lens with strength varying over the bunch length in proportion to the local charge density. For a Gaussian bunch it thus affects most the middle portions (slices) of the bunch and less the end slices, producing a fan-like structure in phase space, each bunch slice contributing one rib of the fan. The effective, geometric emittance of the whole fan is thus much larger than that corresponding to a single slice, as schematically shown in figure 26. It was however recognized early in the 1980s that the linear part of the effect could be compensated by passing the gun output, properly shaped beam through a solenoid followed by an appropriate length drift space [74]: the fan-like distribution folds progressively over until, at the end of the drift, the effective emittance goes through a minimum, corresponding to a partial re-superposition of the various slice emittances. The residual, bunch charge dependent emittance blow-up is due to non-linear force components [75, 76]. Present state-of-the-art e^- RF guns are routinely capable of 2–10 μm normalized emittances at 1–10 nC per bunch [77], still about an order of magnitude larger than required by next generation LC designs. Further improvements will be necessary also on the driving laser side, particularly when pulse shaping, high repetition rates and high power are needed.

To improve on the situation new gun types are being studied, such as pulsed photodiodes [78]. In this device photocathode and anode form essentially a very small gap diode to which sub-ns long, very HF ($\approx$1 GeV m^{-1}) pulses are applied. In a recent paper it is proposed to generate 100 fs, 0.1 nC bunches by accelerating photoelectrons to 2 MeV over a 2 mm gap diode whose anode is the back wall of a standard RF cavity [79]. Because no space charge induced longitudinal emittance blow-up is expected the device could become a good source of (relatively low charge) ultra-short bunches.

Methods to directly produce flat rather than round beams are also being studied. It is for instance shown that a round beam at the cathode can be transformed, into a flat one by using an RF gun, whose cathode is embedded in a solenoidal field $B_{z,c}$, followed by a suitable skew quadrupole triplet [80]. The emittance aspect ratio $r_\varepsilon \equiv \varepsilon_x/\varepsilon_z$ can be adjusted by simply varying $B_{z,c}$. Design studies based on this scheme [81] predict that, $a \approx 1$ nC charge, 100 ps long bunch with $r_\varepsilon > 300$ and $\varepsilon_{nz} \approx 0.03\,\mu$m could be obtained. A very first experimental verification was recently carried out at FNAL where 1 nC bunches with $r_\varepsilon \approx 50$ and $\varepsilon_{nz} = 0.9\,\mu$m were produced [82].

Finally, polarized electron sources are, as of today, produced from semiconductor GaAs photocathodes whose quantum efficiency lifetime is of a few hours only unless they are operated in a vacuum better than $\approx 10^{-10}$ Torr. The specification is not easy to satisfy in high frequency

RF guns because of the intrinsic low pumping conductance of the structure. DC guns, much easier to evacuate, are therefore a promising alternative. Larger, low frequency RF guns and open RF structures like the 'plane wave transformer' [83] are also being proposed but experimental results are still lacking.

Producing positrons with the desired intensity and emittance is much more difficult. Conventional methods via pair production by an e^- beam incident on a high Z target, are only adequate for warm, relatively low average current colliders but not for very high intensity, high beam power superconducting machines. For these a novel scheme has been proposed in which the spent e^- beam after collision is passed in a wiggler magnet [84] in which it radiates creating large numbers of bunched, HE photons that are then converted into e^+e^- pairs in a thin metallic target [85] and captured in a conventional capture and pre-acceleration structure [86].

3.1.4. Very HE LC designs. The choice of the accelerating frequency, gradient, beam power, beam dimensions at the IP, the resulting tolerances and sensitivity to perturbations, and the accelerator upgrade potential of a HE LC, are all very much dependent on the type of RF technology adopted.

The two main approaches on the table are one based on superconducting accelerating structures (TESLA) the other on warm ones (NLC/JLC, CLIC). In both cases work is in progress, in dedicated test facilities, that have been and are producing a wealth of basic and technological knowledge, to fully assess cost and reliability of technical solutions and design parameters extrapolated a long way beyond present experience. In either case, optimizing the overall cost to performance ratio is not straightforward because many entangled parameters are involved.

The main parameters of the three most advanced designs are collected in table 8.

Table 8. TESLA, NLC/JLC and CLIC main parameters.

	TESLA		NLC/JLC		CLIC		
C.m. energy (GeV)	500	800	500	1000	500	1000	3000
RF frequency (GHz)	1.3		11.4		30		
Acceleration gradient (MV m^{-1})	23.4	35	48.5	55	150		
Total site length (km)	33	33	13	30	5	10	30
e^+e^- luminosity (nb s)$^{-1}$	34	58	20	34	14	27	27
$\gamma\gamma$ luminosity (nb s)$^{-2}$	6	—	—	—	—		
Linac pulse length (μs)	950	860	0.27		0.10		
Bunches/pulse	2820	4886	192		154		
Pulse repetition rate	5	4	120		200		
Bunch spacing (ns)	337	176	1.4		0.67		
Particles/bunch, N_b (10^{10})	2	1.4	0.75		0.4		
Pulse repetition rate (Hz)	5		120		200	150	100
β_x, β_y (mm)	15, 0.4		8, 0.11	13, 0.11	10, 0.15		8, 0.15
H_D	2		1.4	1.5	1.8	1.9	2.2
D_x, D_y	0.2, 26		—, 14	—	—	—	—
Collision energy spread (%)	3.2	4.3	4.7		4.4	11.2	31
Bunch length (mm)	0.3		0.1		0.03		
Horizontal rms beam size (nm)	553		245		200	115	43
Vertical rms beam size (nm)	5		2.7		2.5	1.75	1
Two-beam average power (MW)	22.6	34.0	13.8	27.6	9.8	14.8	29.6
Wall-plug to beam efficiency	0.23		0.1		0.10		
Total average wall-plug power (MW)	97	146	140	280	98	148	296

The superconducting approach, chosen for TESLA, is based on relatively low frequency, L-band (1300 MHz) multicell resonators operating at ≈2 K. The design average gradient is 25 MV m^{-1}, eventually upgradeable to ⩾35 MV m^{-1}. Very schematically, a cold structure has higher overall power efficiency η_{RF} because of its higher quality factor Q. A side benefit of the high Q is that the energy stored in the e.m. field $E_{\mathrm{S}} = Q \cdot P_{\mathrm{D}} f_{\mathrm{RF}}^{-1}$ is also large, which can in turn translate into smaller beam energy spread. In addition, for given overall power consumption and frequency, the shape of the cavity can be chosen much more freely, in particular so as to reduce the number of HOMs and their effects on the beam. For same peak field, lower peak power, less expensive klystrons and modulators can be used and, for same overall power consumption, higher currents in longer bunch trains can be accelerated. Long trains make the system more efficient because less power is wasted during the pulse rise and fall times when there is no beam. In addition, bunch spacing can be large, which simplifies the design of the IR and of the detector and allows bunch by bunch beam steering and damping of cavity HOMs. The end result is either a more tolerant machine for given luminosity or higher luminosity for given tolerances and beam sizes.

On the other hand, gradients comparable to those of warm structures are not achievable. The ultimate limit, set by the material critical magnetic field (≈50–60 MV m^{-1} for Nb), does in fact define the upgrade potential of a cold, fixed length accelerator. Great progress on accelerating fields has been made over the past decade, as shown in figure 27, lately mainly in the framework of the TESLA collaboration [87]. Efficient and reliable operation of large installations, CW operation at high power, recirculation, HFs at competitive prices have been demonstrated, opening the road to a wide spectrum of other SC Linac applications ranging from radiation and neutron spallation sources to energy production and waste treatment facilities and even to very HE hadron accelerators.

The goals set for the TESLA project in the mid 1990s to make its cost per unit energy competitive with warm solutions, were: an average field of 25 MV, in actual operation and structure a reduction of the cost per unit length by a factor of ≈4. They were both met in 2001 at the TESLA test facility (TTF), where a 300 MeV Linac equipped with TESLA type cavities is in operation, being upgraded to ≈1 GeV.

The warm approach taken by NLC, JLC [88] and CLIC [89], focuses instead on achieving the highest possible accelerating field and hence the shortest possible accelerator. Because

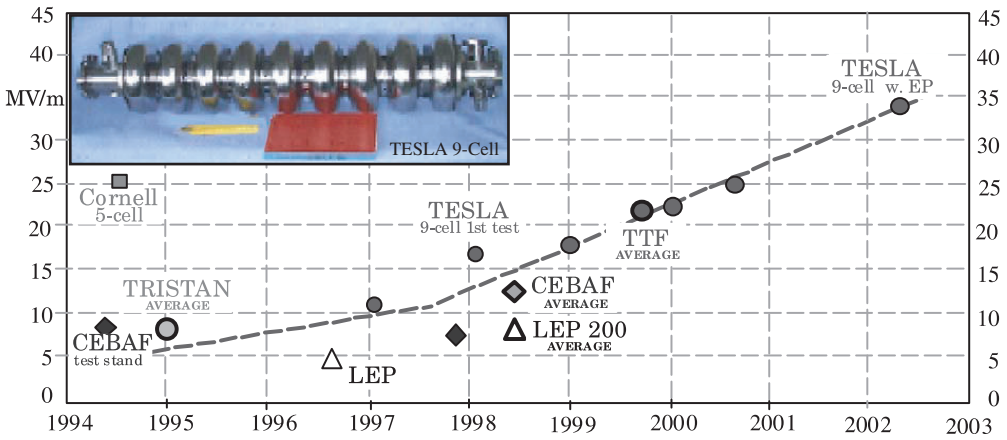

Figure 27. Accelerating fields achieved in superconducting resonators at Cornell, CEBAF, TRISTAN, LEP and TESLA/TTF.

the top field achievable in a given warm structure increases with frequency, high frequencies are favoured. On the other hand, peak and average power dissipation in the structure limit the peak and average accelerated current so that N_b and the length of the bunch train must be smaller.

The structure physical bore, the smaller the higher the frequency, makes for stronger wake fields (equation (3.1.8)) and needs lower emittances. Alignment tolerances, mechanical and electrical stability of all optics and accelerating system components, the latter being the main cause of off-axis beam deflection and hence of transverse wake field excitation, become more stringent, emittance preservation and final focus optics more difficult. Finally, for same luminosity beam sizes must be made and kept much smaller.

In the NLC/JLC case, balancing RF peak power vs gradient, a cost minimum is reached at 11.4 GHz with an unloaded gradient of 70 MV m^{-1} dropping to 50 MV m^{-1} at full load. In this frequency range new klystrons and modulators had to be developed. CLIC, aiming at multi-TeV energies and therefore at even higher gradients, has come up with an unloaded gradient of 170 MV m^{-1} ($\geqslant$80 MV m^{-1} at full load) at 30 GHz, a frequency at which an entirely new RF drive concept, the two-beam scheme [90], had to be devised.

Since beam sizes at the IP depend on the beam emittance $\varepsilon_{x,z}$ (equation (2.1.2)), a problem common to all LCs is preventing emittance from being spoiled during acceleration by the beam interacting with longitudinal, $E_\parallel$, and transverse, $E_\perp$, wake fields excited by the beam in its environment. Wake field intensities scale with RF frequency, f_{RF}, and bunch population approximately like

$$E_\parallel \propto N_b f_{RF}^2 \qquad \text{and} \qquad E_\perp \propto N_b f_{RF}^3. \tag{3.1.8}$$

Transverse short-range wake fields can distort the bunch shape or provoke single-bunch instabilities. Because they are excited by the beam passing off-axis, maintaining tight tolerances on orbit deviations over very long distances, in the presence of e.m. noise and mechanical vibration, is a main concern [91].

Transverse resonant HOMs, excited by a given bunch in high Q resonators, can also affect the trailing bunches causing multibunch instabilities. Large bunch spacing helps reducing their effect. Finally, longitudinal short-range wake fields mainly produce bunch energy spread and chromatic emittance dilution [92].

The wake fields steep scaling with frequency (equation (3.1.8)) greatly favours low frequencies and therefore superconducting structures. It has however been recently pointed out [93] that by careful tuning of quantities such as bunch length, focusing optics parameters, RF structure alignment tolerances and N_b, all influenced by the RF frequency and having strong influence on emittance degradation, the final emittance and energy spread frequency dependence can be significantly reduced.

Achieving the nanometre spot sizes at the IP, required by present LinC designs imposes severe constraints on the collider final-focus system (FFS) that operates like a demagnifying telescope: small beam sizes require large demagnification factors that in turn call for very strong focusing and large aperture final focus quadrupolar lenses. Large chromatic aberrations must consequently be carefully corrected to allow focusing beams that typically have a relative energy spread of $\approx$0.1% [94].

Figure 28 shows the TESLA layout scheme. The very long damping rings are needed to accommodate the (compacted) 0.8 ms long Linac pulse. The basic accelerating structure module is a 15 m long cryostat containing eight 9-cell, 25 MV m^{-1} Nb cavities, a focusing quadrupole and corrector elements. For 500 GeV c.m., over 20 000 9-cell cavities will be needed. By raising the accelerating gradient to $\approx$35 MV m^{-1}, a value already achieved on prototype 9-cell cavities, TESLA can be upgraded to 800 GeV c.m.

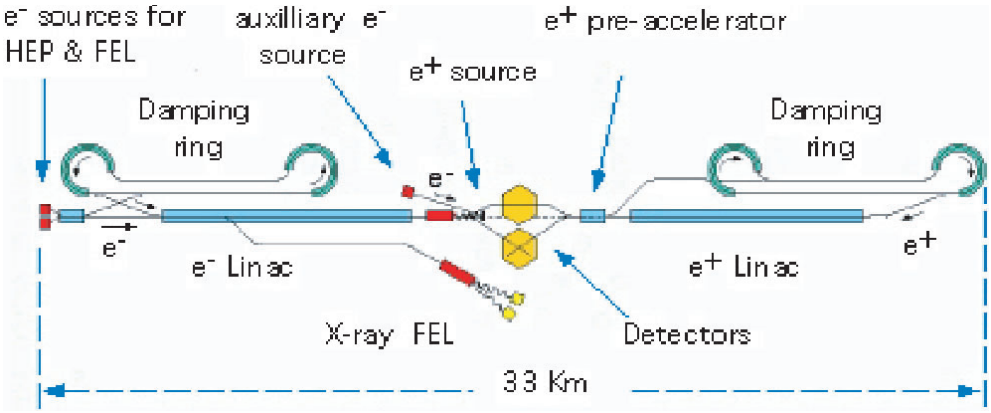

Figure 28. Simplified layout of the TESLA design.

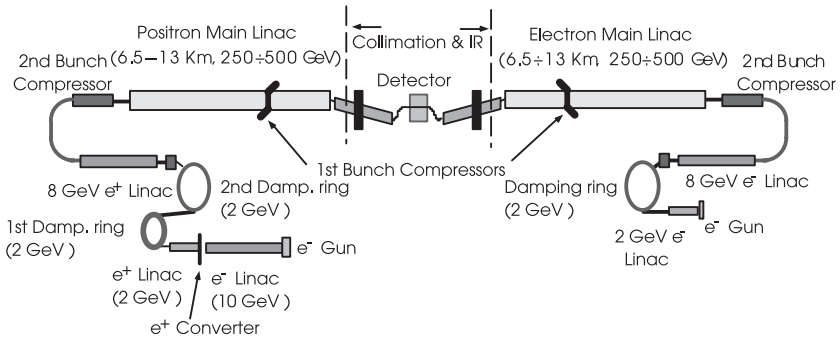

Figure 29. Simplified layout of the NLC/JLC design.

A new scheme including a 2×7-cell basic cavity, a simplified cavity powering arrangement and a somewhat higher filling factor, is also being tested [95].

The layout of the NLC/JLC designs is not substantially different (figure 29) but its damping rings are much shorter since the pulse train length supported by NC structures is only 267 ns long. The very high peak power to be fed to the structure has required developing new klystrons and complicated powering schemes. The tunnel length is such that the initial 500 GeV c.m. design energy can be upgraded to 1 TeV by doubling the number of accelerating structures and the number of klystrons.

A problem connected with surface damage of the copper accelerating structures has recently come up while testing long term operation at gradients in excess of $50\,\mathrm{MV\,m^{-1}}$ [96] in the SLAC NLCTA test facility. The problem is being studied and possible solutions suggested [97, 98].

The CLIC design (figure 30) is conceptually different. Aimed at energies well in excess of 1 TeV it would operate at a gradient of $\geqslant 80\,\mathrm{MV\,m^{-1}}$ and 30 GHz, a band where no known suitable power sources exist. RF power is therefore generated in a novel manner, as schematically indicated in figure 30. The relatively low energy bunch train of an L band (937 MHz) normal conducting Linac carries all the necessary average power. Through an arrangement comprising a bypass and two storage rings, the bunch spacing is reduced so that a new bunch train with a main Fourier component at 30 GHz, with appropriate peak power is

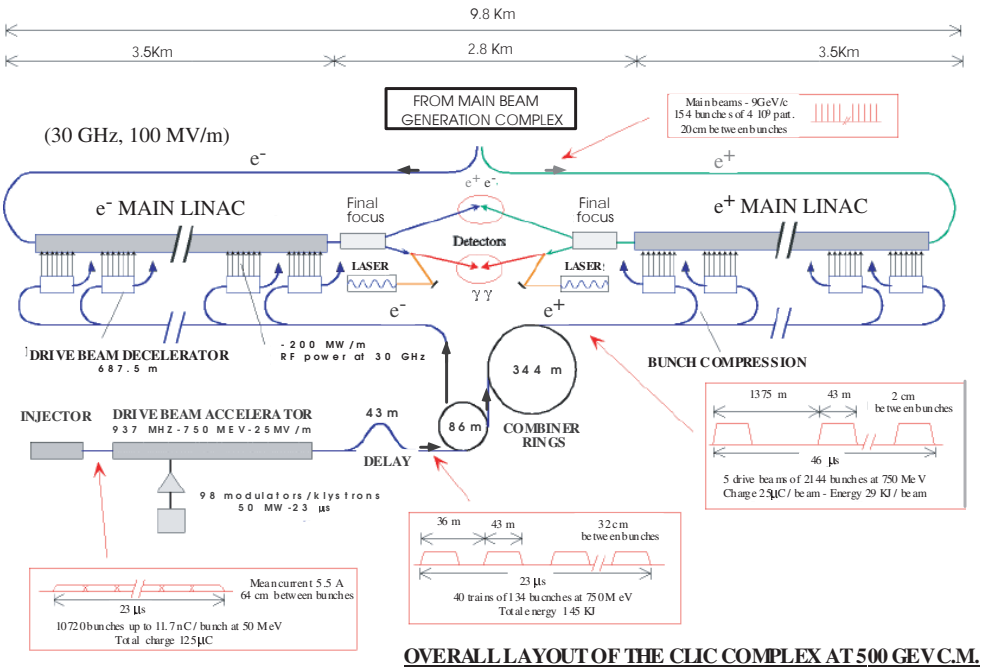

Figure 30. Simplified layout of the CLIC complex design layout.

produced. The so obtained train is also segmented and timed in such a way that each segment can be passed through an appropriate decelerating structure that extracts its power in the form of a 30 GHz e.m. pulse and finally feeds it to the main accelerating structures in coincidence with the passage of the main beam pulse to be accelerated [89].

3.1.5. Novel acceleration techniques. The most important practical limitation that HE colliders face today is the cost per GeV of beam energy.

One way of attacking the problem is to investigate how present RF technology and accelerator design could be upgraded. Schemes on how to design a 5 TeV c.m. collider with 100 $(\text{nb s})^{-1}$ luminosity by improving and upgrading 'conventional' techniques are discussed in [99]. In [100] the same author discusses in more detail how accelerating gradients of $\approx$1 GeV m^{-1}, two orders of magnitude higher than present ones could be achieved, possibly even with warm copper structures, by operating at frequencies as high as 140 GHz, a frequency at which a high power generator based on a FEL, was put in operation in 1993 [101]. Along the same line of thought, a 'sample design' of a 5 TeV collider only 10 km long and using only 12 MW of beam power is presented in [102].

Other advanced accelerator techniques, such as plasma or laser based acceleration, that promise gradients ranging from several 100 MV m^{-1} up to 150 GV m^{-1}, would allow for ultra-compact LCs in the multi-TeV range [103]. More exotic schemes have therefore been proposed, studied and researched, mainly over the past two decades, based on the idea of utilizing for acceleration the very HFs generated in plasmas or in vacuum by high power lasers or by auxiliary particle beams, or in laser excited dielectric resonant structures, etc. (There is clearly a 'symbiotic relationship' between future accelerators, synchrotron light sources and lasers.)

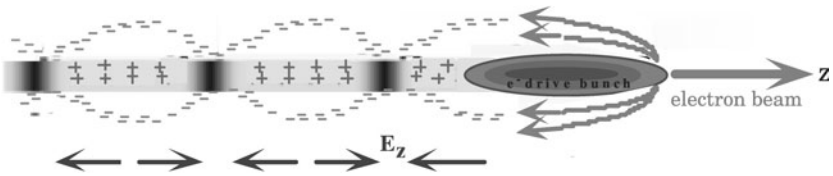

Figure 31. Plasma acceleration principle.

An interesting story, by one of the plasma accelerator founding fathers, on how the idea was born and developed can be found in [104]. The laser/plasma-based approach received a strong boost by the end of the 1980s when chirped pulse amplification and progress in mirror and beam handling techniques in general, produced TW tabletop lasers. Peak powers today reach up to 100 TW with focused intensities of the order of $\approx 10^{20}\,\mathrm{W\,cm^{-2}}$ [105]. In a vision of the future that contemplates intensities of the order of $10^{26}\,\mathrm{W\,cm^{-2}}$, corresponding to gradients of $200\,\mathrm{TeV\,cm^{-1}}$, some authors estimate that very bright, 100 TeV, sub-picosecond intense electron pulses could be produced. A panorama of what this scenario could bring for QED and hot matter studies and for applications such as fusion and ion acceleration is also outlined [105]. A review of the present status of laser-plasma accelerators is given in [106].

The principle of the most popular electron-beam-driven plasma wake field acceleration (PWFA) scheme is illustrated in figure 31. A plasma channel is generated in a neutral gas by ionizing it with a laser. By then passing a leading, high charge e^- bunch through the channel the negative charges are displaced leaving charge oscillations in their wake. A trailing, lower charge bunch, injected in the resulting longitudinal wake field with the right phase, can thus be accelerated. Accelerating gradients up to $160\,\mathrm{GV\,m^{-1}}$ have been measured [107] in a 0.6 mm long plasma.

Plasma oscillation wavelength and longitudinal field value can be estimated to be

$$\lambda_\mathrm{p} \approx \sqrt{\frac{10^{15}\,\mathrm{cm^{-3}}}{n_0}}\ (\mathrm{mm}) \qquad \text{and} \qquad E_z \approx 100\sqrt{n_0}\ (\mathrm{V\,m^{-1}}), \tag{3.1.9}$$

respectively, n_0 being the plasma density. The equations show that bunches to be accelerated must be rather short: as an example, with $n_0 = 10^{14}\,\mathrm{cm^{-3}}$ one has $\lambda_\mathrm{p} = 3.3\,\mathrm{mm}$ and $E_z = 1\,\mathrm{GV\,m^{-1}}$. Femto-second long bunches should thus be injected with sub-fs timing accuracy.

As much as recent results are encouraging and progress is being made on the active length of the plasma—a 1.4 m long plasma is reported to have been obtained that provides an energy gain of 150 MeV [108]—the main problems still remain, at least for HE and light-source applications, of controlling and preserving the bunch quality over reasonable distances in a plasma environment, so that an actually operable HE facility (at present much beyond the state-of-the-art) could be considered [109].

Nevertheless, interesting if daring approaches to the problem of designing (or upgrading) accelerators using such acceleration techniques have been presented. In [110] it is for instance proposed to use the PWFA technique for a 1.2 TeV, $\approx 0.5\,\mathrm{GeV\,m^{-1}}$, e^-e^- or $\gamma\gamma$ collider. Six-metre long plasma modules are driven by a single 3 GeV, L-band normal conducting Linac that provides both the leading and the trailing bunches. Modules work in the extreme non-linear, 'blow-out' regime, in which all electrons are effectively swept from the beam path and the positive ions provide transverse focusing. Results from numerical simulations and possible drive beam and plasma module parameters are given.

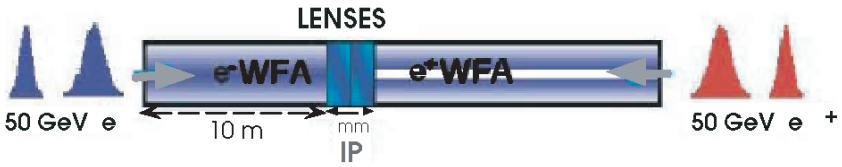

Figure 32. Schematic layout proposed for doubling the energy of the SLC [112].

The idea of using a hollow plasma channel in the blowout regime to raise the present SLC energy is taken up again in [111, 112]. The latter, more 'conservative', paper is based on detailed three-dimensional numerical calculations of wake fields and beam dynamics.

3 nC drive bunches would be generated by the present SLAC Linac and longitudinally compressed, by about a factor of 10, to $\approx$60 μm length. The trailing bunch would be accelerated at a computed 8 GeV m^{-1} rate over a 7 m long plasma cell, totalling $\approx$56 GeV and thus doubling the present SLC energy. The computed relative bunch energy spread is 20%. Luminosity is recovered by squeezing down the colliding beams at the IP by means of two plasma lenses next to the IP. A schematic layout is shown in figure 32.

A number of serious problems are recognized by the authors: the required transverse bunch size must be $\approx$1 μm which is below present resolution of beam dynamics 'particle-in-cell' simulation programs, stability problems require studying, the actual feasibility and operability of the final focus plasma lenses as well as the implementation of the required PWA plasma parameters are open questions, interactions with the experimental detector have not been considered. The attempt to accelerate both electrons and positrons is even more complicated. The figure indicates schematically that for this reason the two sides of the apparatus cannot be identical.

Other acceleration schemes such as the laser injected linear accelerator (LILAC), an 'all-optical' injection system devised to trap and accelerate ultra-short electron bunches, are also being considered. LILAC is claimed capable of GeV cm^{-1} gradients, micrometre spot sizes, 1 fs long bunches and 1 GeV cm^{-2} current densities [113]. Electrons are injected into the wake field of a plasma wave generated by the first of two orthogonal laser beams illuminating a confined gas. The first laser (drive) pulse ionizes the gas creating a plasma wave with amplitude lower than its self-trapping threshold, meaning that electrons oscillate freely around ions. The transverse ponderomotive force of the second (injection) orthogonal laser pulse imparts to the plasma electrons an extra kick in the wave direction, injecting them into the drive pulse wake with the correct phase to be trapped and accelerated [114].

3.2. Muon accelerators

3.2.1. Muon colliders. Circular muon colliders (MuC), free from the limitations set by SR and beamstrahlung, promise energies in the multi-TeV range and luminosities in excess of 10 (nb s)$^{-1}$. The installation size would be very much smaller than that of comparable energy *ee* ones (figure 35), which is expected to result in significantly lower costs per GeV.

The production and acceleration of bright enough beams of unstable particles with rest frame lifetime, τ_μ, of only 2.2 μs, however, poses a number of serious technical problems. The feasibility of such colliders, while being actively studied in Europe, the USA and Japan, remains therefore to be proven.

A typical layout scheme is shown in figure 33. The muon source is based on a high-intensity proton (linear or circular) accelerator complex that generates short, intense proton

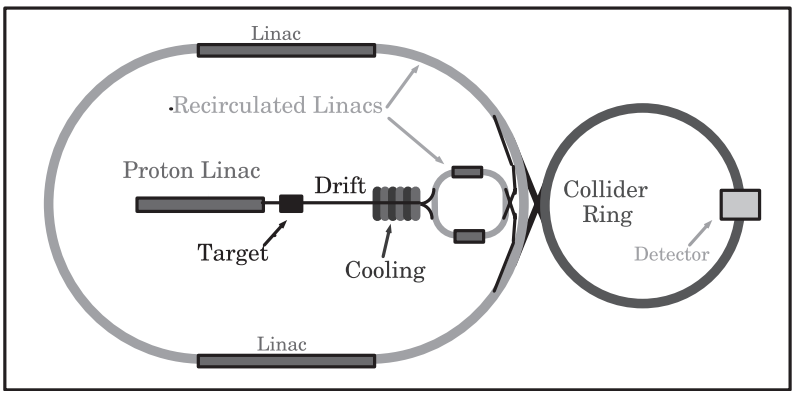

Figure 33. A possible muon collider layout scheme.

pulses. These are fired onto a high Z target to produce large numbers of $\pi^{\pm}$ mesons, which are then captured either in a magnetic horn or in a high field solenoid in which the target is immersed. Because several MW of protons are needed, new types of targets, such as heavy liquid jet devices of the kind to be used in large spallation sources, will be needed. Alternative arrangements comprising multiple targets to reduce the power per target are also being proposed [115]. The muon source is followed by a long straight section, immersed in a solenoidal field adiabatically matched to a magnetic field arrangement in which the $\pi^{\pm}$ mesons drift long enough to essentially all decay to $\mu^{\pm}$. The drift section also contains a low frequency RF system that captures the muons, bunches and pre-accelerates them and rotates the bunches in longitudinal phase-space so as to reduce the ≈100% initial beam energy spread at the expense of bunch length.

The captured muon beam transverse emittance is at this stage of order 1 m rad, 10^5–10^6 times larger than required for the kind of luminosities being considered. The most promising method to reduce it is cooling by ionization: muons are passed through a number of stages each consisting of an absorber in which particles are scattered losing both transverse and longitudinal momentum, followed by an RF cavity that re-accelerates them to their initial energy by boosting their longitudinal momentum only. The transverse emittance is thus reduced.

The beam energy spread should also be simultaneously reduced to its final ≈5% specification by introducing a correlation between the particle energy and its transverse position and by appropriately grading, as a function of transverse position, the absorber thickness (or density). The cooling process eventually reaches an equilibrium determined by stochastic heating due to multiple scattering processes. Whether the needed large cooling factor can actually be obtained is one of the major question marks. A sketch layout of the MICE experiment [116], being planned by an international collaboration to test the performance of a cooling channel basic elements, is shown in figure 34.

Other serious problems still to be solved are connected with the very high radiation levels to which major accelerator components are exposed, with environmental radiation hazards and, on the detectors side, with the 'huge muon and electron backgrounds'. While, as mentioned earlier, the feasibility of such facilities is being investigated both theoretically and experimentally, it will probably be some time before an actual technical design report can be confidently produced.

Cooled μ^+ and μ^-bunches must then be accelerated to their final energy in a time short compared to τ_μ by a sequence of accelerators (recirculated Linac as in figure 33, Linacs,

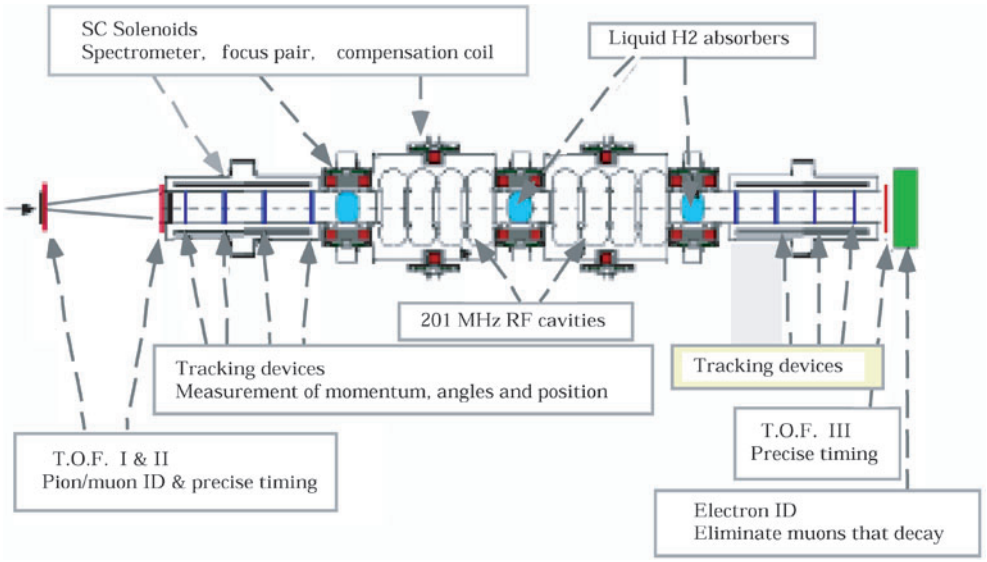

Figure 34. Sketch of the MICE cooling experiment. Liquid hydrogen absorbers will be used.

synchrotrons) devised to minimize cost, and finally injected into a circular collider ring in which they are kept coasting and colliding for a time of the order of τ_μ.

The fraction $(N_\mu/N_{0\mu})$ of μ's surviving acceleration from the initial energy $E_{\rm in}$ to the final E is

$$\left(\frac{N_\mu}{N_{0\mu}}\right) = \left(\frac{E}{E_{\rm inj}}\right)^{(m_{0\mu}c^2/L_\mu)/E}, \tag{3.2.1}$$

$L_\mu = c\tau_\mu = 660\,\text{m}$ being the muon decay length and E the accelerating field. A modest $3\,\text{MeV}\,\text{m}^{-1}$ field is sufficient to accelerate 70% of the muons to 1000 times $E_{\rm in}$. For highest luminosity, the collider ring circumference C should be the shortest possible, the number of turns in a lifetime, independent of energy, being simply $n_\tau = (c/C)\cdot\tau_\mu$

Assuming the beta functions at the IP are made equal and equal to the bunch length σ_y^*, the luminosity of a round Gaussian beam with rms radius σ and rms energy spread ΔE can be written as a function of the longitudinal and transverse normalized emittances as follows [117].

$$L_{\mu\mu} = \frac{\langle N_\mu^2\rangle H_{\rm D}}{4\pi(\sigma^*)^2}\cdot f_{\rm rep} \cong \frac{\langle N_\mu^2\rangle}{4\pi}\cdot\frac{\gamma}{\varepsilon_{n\perp}\beta^*}\cdot f_{\rm rep} = \frac{N_\mu^2}{4\pi}\frac{\gamma^2\Delta_E}{\varepsilon_{n\perp}\varepsilon_{n\parallel}}\cdot f_{\rm rep}, \tag{3.2.2}$$

having set $H_{\rm D}\approx 1$ and $\beta^*\cong\sigma_y^* = \varepsilon_{n\parallel}/(\gamma\,\Delta E)$. Given that the minimum achievable bunch length, and hence the value of β^*, is in practice of a few hundred μm, the last expression shows that luminosity essentially depends on the normalized limit value of the cooled $6D$ emittance $\varepsilon_{n6}\approx\varepsilon_{n\perp}\varepsilon_{n\parallel}$.

The approximate sizes of different energy muon collider designs and of the highest energy e^+e^- and proton colliders are compared in figure 35.

Preliminary design parameters, recently published [118], are listed in table 9.

3.2.2. Neutrino factories. Because muons decay to electron plus neutrino, a muon beam with energy in the 50 GeV range and intensity close to that foreseen for a collider would produce a neutrino flux orders of magnitude higher compared to more standard fixed target sources and,

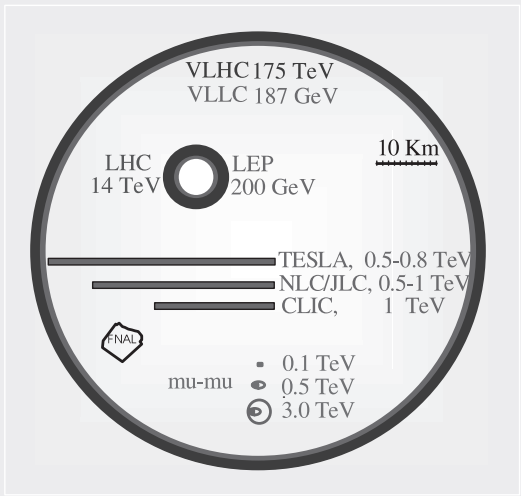

Figure 35. Relative sizes of the highest energy colliders, in construction (LHC) or proposed. (Red (large and small inner rings and centre) e^+e^-, blue (large and small outer rings) pp, green (bottom) muon colliders.) The size of the FNAL site is also shown.

Table 9. Muon collider tentative parameters.

Energy (TeV)	3	0.1
Luminosity ($\mathrm{cm}^{-2}\,\mathrm{s}^{-1}$)	7×10^{34}	2.2×10^{31}
Circumference (km)	6	0.35
N_μ	2×10^{12}	4×10^{12}
Δ_E (%)	0.16	0.01
$6D\ \varepsilon_{n,6}$ (π m)^3	1.7×10^{-10}	1.7×10^{-10}
ε_n (π mm mrad)	50	195
β^* (cm)	0.3	9.4
P_{AC} (MW)	204	81

in addition, neutrino pairs consisting of a μ-type ν and an e-type $\bar{\nu}$ (or vice versa), thereby opening up a whole new class of neutrino physics experiments. The beam quality required from such a single-beam neutrino factory would on the other hand set much less stringent requirements than a collider on the muon beam parameters, and in particular on its emittance. Because it would serve to gradually perfect the technology while at the same time supporting extremely interesting physics programmes, it is seen as a most desirable first step towards a muon collider.

A schematic layout of such a neutrino factory designed at CERN is shown in figure 36 [119]. Up to the final stage the scheme is the same as for the collider but with much relaxed specifications. The muon beam is accelerated to 50 GeV by two recirculated Linacs and finally injected into a storage ring with very long decay straight sections from which well-directed intense neutrino beams are extracted. Studying neutrino oscillations requires sending the beams on to far away detectors, the different 'baselines' ranging from ≈500 to ≈8000 km.

The figure-of-8-ring shape of the final storage ring is such as to aim the muon beams directly at existing far away neutrino laboratories. A new problem for the accelerator designer is to the incline the different straight sections with respect to the surface of the Earth, depending on the desired baseline length and the location of the end detector.

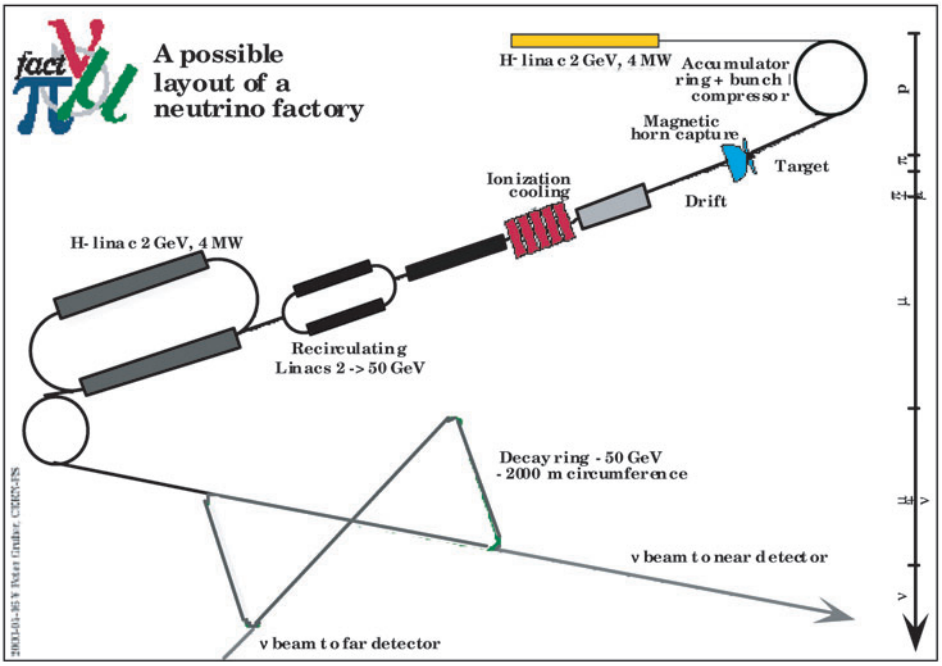

Figure 36. Layout of the CERN neutrino factory scheme.

References

N.B.: Full text proceedings of all major international accelerator conferences (EPAC, PAC, LINAC, APAC) since 1995 can be found at the joint accelerator proceedings site, http://www.cern.ch/accelconf/top-page.html. In the following only the paper ID code is therefore given (e.g. FBC001 for [1]) instead of the full web address.

[1] Peoples J 1997 Future directions of high energy physics *Proc. PAC* FBC001
[2] Ellis E, Keil E and Rolandi G 1998 Options for future colliders at CERN *CERN Int. Rep.* CERN-SL-98-004
[3] Kerst D W *et al* 1956 Attainment of very high energy by means of intersecting beams of particles *Phys. Rev.* **102** 590–1
[4] De Roeck A *et al* 2001 Physics motivations for future CERN accelerators *Int. Rep.* CERN-TH/2001-023
[5] Ostojic R 2001 Status and challenges of the LHC construction *Proc. PAC01* Chicago MOPA002
[6] Willeke F 2002 HERA status and perspectives of future Lepton–Hadron colliders *Proc. EPAC* TUYGB001
[7] Antinori F *et al* 2000 Enhancement of strange and multi-strange baryons in central Pb–Pb interactions *Nucl. Phys.* A **663–664** 717
[8] Ozaki S 2001 RHIC commissioning and first results *Proc. PAC* MOAL001
[9] The STAR Collaboration 2002 Results from the STAR experiment *Nucl. Phys.* A **698** 64c–77c
[10] Erickson R (ed) 1994 *SLC Design Report* SLAC-PUB
[11] Autin B 2000 Technical challenges of neutrino factories *Nucl. Instrum. Methods* A **451** 244
[12] Brandt D 2000 Accelerator physics at LEP *Rep. Prog. Phys.* **63** 939–1000
[13] Zimmermann F 2001 Luminosity limitations in Hadron colliders *Int. Rep.* CERN SL-2001-009 AP
[14] Keil E and Talman R 1982 Scaling of luminosity data between e^+e^- storage rings *LEP Note* 387
Zimmermann F 2002 Accelerator physics issues at the LHC and beyond *CERN Int. Rep.* CERN SL-2002-003 AP
[15] Ambrosio *et al* 2001 VLHC accelerator physics *FNAL Int. Rep. TM-2158* http://vlhc.org/AP.pdf
[16] Herr W and Ruggiero F 1999 Summary of the workshop on beam–beam effects in large Hadron colliders (LHC99) *LHC Proj. Rep.* 277
[17] Benvenuti C, Circelli N and Hauer M 1984 *Appl. Phys. Lett.* **45** 583
Hübner K 2001 The LEP superconducting RF system *Int. Rep.* CERN SL-2001-059
[18] Padamsee H 2001 Superconducting RF—new directions *Proc. PAC* ROAA001

[19] Tigner M 1965 A possible apparatus for electron clashing-beam experiments *N. Cim.* **37** 1228
[20] Amaldi U 1976 A possible scheme to obtain e^-e^- and $e^{+-}e^-$ collisions at energies of hundreds of GeV *Phys. Lett.* **61B** 313
[21] Sen T and Norem J 2001 A very large Lpton collider in the VLHC tunnel *Phys. Rev. ST AB* **5** 03
[22] Guiducci S *et al* 2001 Status report on DAFNE *Proc. PAC* WOAB006
[23] Cai Y *et al* 2001 Status and future plans of the PEP II factory *Proc. PAC* RPPH137
[24] The CLEO-c Collaboration 2001 CLEO Project Description, http://www.lns.cornell.edu/public/CLEO/spoke/CLEOc/ProjDesc.html
[25] Oide K 2002 Operation experience and performance limitations in e^+e^- Factories *Proc. EPAC* MOXGB002
[26] Zimmermann F and Rumolo G 2001 Two-stream problems in accelerators *Int. Rep.* CERN SL-2001-057 (AP)
[27] Gröbner O 1998 Beam induced multipacting *Proc. EPAC* MOP10C
[28] Fox J *et al* 1998 Multi-bunch longitudinal dynamics and diagnostics via a digital feedback system at PEP-II, Dafne, ALS and SPEAR *Proc. EPAC* WEOB01A
Bulfone D 2002 The ELETTRA digital multi-bunch feedback systems *Proc. EPAC* Paris (Fr), THPRI035
[29] Padamsee H 1998 Review of experience with HOM damped cavities *Proc. EPAC* THX02B
[30] Boni R 1996 HOM-free cavities *Proc. EPAC* TUY01A
[31] Oide K 2002 Operation experience and performance limitations in e^+e^- factories *Proc. EPAC* MOXGB002
[32] Seeman J 2001 Higher luminosity B-factories *Proc. PAC* WOAA003
[33] Emery L 2001 Recent operational data on continuous top-up operation at the advanced photon source *Proc. PAC* WPPH064
[34] Wu Y Z 1997 Beijing tau-charm factory deign study *Proc. PAC* 6B011
[35] McGinnis D 2000 Tevatron collider luminosity upgrades, http://www–bd.fnal.gov/hq/DOE_2000_McGinnis/DOE_McGinnis/
[36] The LHC Study Group 1995 The LHC conceptual designreport *Int. Rep.* CERN/AC/95-05
[37] Benda V *et al* 1996 Conceptual design of the cryogenic system for the LHC *Proc. EPAC* THO04A
[38] Cruikshank P *et al* 1997 Mechanical design aspects of the LHC beam screen *Proc. PAC* 4P003
[39] Bordry F *et al* 2001 Machine protection for the LHC: architecture of the beam and powering interlock systems *LHC Project Report* 521
[40] Mokhov N V and Rakhno I L 2001 Protecting LHC components against radiation resulting from colliding beam interactions *Proc. PAC* RPAH135
[41] Courtesy of L Rossi, CERN
[42] Modena M *et al* 2001 Final prototypes, first pre-series units and steps towards series production of the LHC main dipoles *Proc. PAC* TOAB003
[43] Scandale W *et al* 1998 Field-shape imperfections of the CERN-LHC dipole arising from mechanical deformations and component tolerances *Proc. EPAC* TUP13H
[44] Gareyte J 1999 Beam–beam design criteria for LHC *CERN Int. Rep.* CERN-SL-99-039
[45] Herr W and Ruggiero F 1999 Summary of the workshop on beam–beam effects in large Hadron colliders (LHC99) *LHC Proj. Rep.* 277
[46] Herr W 1996 Effects of PACMAN bunches in the LHC *LHC Proj. Rep.* 39
Jowett J 1999 Collision schedules and bunch filling schemes in the LHC *LHC-Project–Note-179*
[47] Grote H 1999 Beam–beam effects in the LHC *CERN Int. Rep.* CERN-SL-99-039-AP
[48] Koutchouk J P 2001 Principle of a correction of the long-range beam–beam effect in LHC using electromagnetic lenses *Proc. PAC* TPPH012
[49] Shiltsev V *et al* 1999 Considerations on compensation of beam–beam effects in the Tevatron with electron beams *Phys. Rev. ST- AB* **2** 071001
[50] Zimmermann F 2002 Two-stream effects in present and future accelerators *Proc. EPAC* THZGB001
Zimmermann F 2002 Accelerator physics issues at the LHC and beyond *Int. Rep.* CERN-SL-2002-003 (AP)
[51] Brüning O *et al* 1999 Electron cloud and beam scrubbing in the LHC *Proc. PAC* THA6
[52] Ruggiero F *et al* (ed) 2002 *Proc. ECLOUD'02 Workshop* CERN, http://slap.cern.ch/collective/ecloud02/proceedings/index.html
[53] *Proc. LHC IR Upgrade Collaboration Meeting (March 2002)* http://lhc-proj-ir-upgrade.web.cern.ch/lhc-proj-IR-upgrade/
[54] Taylor T M 2002 Superconducting magnets for a super LHC *Proc. EPAC* MOYGB002
[55] Gourlay S 2001 Fabrication and test of a high field Nb_3Sn superconducting racetrack dipole magnet *Proc. PAC* TOAB009
[56] Courtesy of S Gourlay, Berkeley National Laboratory, CA, USA
[57] Takayama K *et al* 2002 Induction accelerating devices for induction synchrotrons and the superbunch VLHC *Proc. PAC* MOPRI075

[58] Ruggiero F and Zimmermann F 2002 Luminosity optimization near the beam–beam limit by increasing bunch length or crossing angle *Phys. Rev. ST* A&B **5** 061001
[59] Takayama K *et al* 2002 Superbunch Hadron collider *Phys. Rev. Lett.* **88** 144801
[60] Derrick M *et al* 1999 An e–p collider with Ecm = 1 TeV in a VLHC booster tunnel *Proc. PAC* THA10
[61] Harrison M 1995 The RHIC project—status and plans *Proc. PAC* MPG03
[62] Ozaki S 2001 RHIC commissioning and first results *Proc. PAC* MOAL001
[63] Brandt D 2000 Review of the LHC ion program *Int. Rep.* LHC- Project-Report-450
[64] Chanel M 2001 Ion accumulation for LHC *Int. Rep.* CERN/PS 2001-054
[65] The STAR Collaboration 2002 STAR images *Nucl. Phys.* A **698** 64c–77c, http://www.star.bnl.gov
[66] Peggs S 1999 RHIC status *Proc. LHC99 Workshop* http://www.pubs.bnl.gov/pubs/documents/19297.pdf
[67] Derbenev Ya S 2000 Prospects of high energy electron cooling *Proc. EPAC* MOZE03
[68] Ben-Zvi I *et al* 2001 Electron cooling for RHIC *Proc. PAC* MOPA01
[69] Alexandrov V A 1995 Results of final focus test beam *Proc. PAC* Dallas, TAGO1
[70] Schulte D 1997 Study of electromagnetic and Hadronic background in the TESLA IR *TESLA-Report* 08
[71] Yokoya K 2000 Beam–beam interaction in linear collider *Proc. Joint USA/CERN/JP/Ru Acc. Sch. High Quality Beams* (AIP) p 592
[72] Takahashi T 2000 Gamma-gamma collider *Proc. 7th Int. Workshop on HE Photon Coll. (Hamburg)* Heuer R D *et al* (ed) 2001 *Nucl. Instrum. Methods* A **472**
[73] Boscolo I and Michelato P 2000 Photocathodes: the state of the art and some news *NIM* A **445** 389–93
[74] Carlsten B E 1989 New photoelectric injector design for the Los Alamos National Laboratory XUV FEL accelerator *Nucl. Instrum. Methods* A **285** 313
[75] Anderson G and Rosenzweig J B 2000 Nonequilibrium transverse motion and emittance growth in ultrarelativistic space-charge dominated beams *Phys. Rev. ST* AB **3** 09420
[76] Serafini L and Rosenzweig J B 1997 Envelope analysis of intense relativistic quasilaminar beams in rf photoinjectors: a theory of emittance compensation *Phys. Rev.* E **55** 7565
[77] Rosenzweig J B and Colby E 1995 Charge and wavelength scaling of RF photoinjector design *DESY Int. Rep.* TESLA-95-04
[78] Srinivasan-Rao T *et al* 1999 Simulation, generation and characterization of high brightness electron source at 1 GV/m gradient *Proc. PAC* MOCR3
[79] de Loos M J *et al* 2002 A high-brightness pre-accelerated RF photo-injector *Proc. EPAC* TUPRI061
[80] Brinkmann R, Derbenev Ya, Flöttmann K 2000 A flat beam electron source for linear colliders *Proc. EPAC* THP3B06 and *DESY Int. Rep.* TESLA-99-09
[81] Brinkmann R, Derbenev Ya and Flöttmann K 2000 A low emittance, flat beam electron source for linear colliders *Proc. EPAC* THP3B06
[82] Edwards D *et al* 2000 The flat beam experiment at the FNAL photoinjector *Proc. LINAC* MOB13
[83] Clendenin J E 1998 Polarized RF gun *Proc. VIII Advanced Acc. Concepts (Baltimore: AIP)* p 472 and SLAC-PUB-7854
[84] Flöttmann K 1999 Positron sources: conversion of undulator radiation *Handbook Acc. Physics and Engineering* ed A W Chao and M Tigner (Singapore: World Scientific)
[85] Ecklund S 1999 Positron sources: tungsten target *Handbook Acc. Physics and Engineering* ed A W Chao and M Tigner (Singapore: World Scientific)
[86] Balandin V V *et al* 2000 The positron injector linac for TESLA *Proc. EPAC* THP3B09
[87] TESLA Technical Design Report 2001 *DESY Int. Rep.* 2001-011, http://tesla.desy.de/new_pages/TDR_CD/start.html
[88] Takata K 2002 Overview of the NLC/JLC collaboration *Proc. XXI LINAC Conf. (Korea, 19–23 August)* http://linac2002.postech.uc.kr/dh/abstract/show_program.php
[89] Corsini R 2002 Overview of CLIC and CTF3 *Proc. XXI LINAC Conf. (Korea, 19–23 August)* at press
[90] Sessler A M and Yu S S 1987 Relativistic Klystron two-beam accelerator *Phys. Rev. Lett.* V **58**
[91] Seryi A 2000 A shaky road to subnanometer beams. NLC ground motion, vibration and stabilization studies *Proc. Ground Motion Workshop* SLAC, http://www.slac.stanford.edu/cgi-wrap/getdoc/slac-wp-018-ch01-Seryi1.pdf
[92] Mosnier A 1993 Instabilities in LINACs *Proc. V CERN Adv. Acc. Phys. Course* CERN Yellow Rep. 95-06
[93] Delahaye J P, Guignard G, Raubenheimer T and Wilson I 1999 Scaling laws for e^+e^- linear colliders *Nucl. Instrum. Methods* PR A **421** 369–405
[94] Raubenheimer T O and Zimmermann F 2000 Final-focus systems in linear colliders *Rev. Mod. Phys.* **72** 95
[95] Sekutowicz J, Ferrario M and Tang Ch 1999 Superconducting superstructure for the TESLA collider: A concept *Phys. Rev.* ST AB **2** 062001
[96] Adolphsen *et al* 2001 Processing studies of x-band accelerator structures at the NLCTA *Proc. PAC* ROAA003

[97] Wilson P B 2001 Frequency and pulse length scaling of RF breakdown in accelerator structures *Proc. PAC* ROAA012
[98] Miller R H 2001 Room temperature accelerator structures for linear colliders *PAC* FPAH062
[99] Whittum D H 1998 New concepts for a compact 5 TeV collider *Proc. EPAC* WEP22G
[100] Whittum D H 1998 SLAC-PUB-7910, http://www.slac.stanford.edu/cgi-wrap/getdoc/slac-pub-7910.pdf
[101] Allen S L *et al* 1993 *Proc. PAC* (New York: IEEE)
[102] Zimmermann F 1998 SLAC-PUB-7883, http://www.slac.stanford.edu/cgi-wrap/getdoc/slac-pub-7883.pdf
[103] Assmann R W 2002 Review of ultra high-gradient acceleration schemes, results of experiments *Proc. EPAC* MOZGB004
[104] Dawson J M 2001 *Proc. Adv. Acc. Concepts 9th Workshop* ed P L Colestock and S Kelley, IOP CP, vol 569, p 3
[105] Tajima T and Mourou G 2002 *Phys. Rev.* ST AB **5** 031301, http://prst–ab.aps.org/pdf/PRSTAB/v5/i3/e031301
[106] Joshi C 2001 *Proc. Adv. Acc. Concepts 9th Workshop* ed P L Colestock and S Kelley, IOP CP, vol 569, p 85
[107] Gordon D *et al* 1988 *Phys. Rev. Lett.* **80** 2133
[108] Muggli P *et al* Review of applications to plasma accelerators *Proc. ICFA Workshop 'Phys. and Appl. of High Brightness Electron Beams' (July 2002, Chia Laguna)* http://www.physics.ucla.edu/AABD
[109] Hoffman J R *et al* 2001 On the possibility of a 10^{16} cm^{-3} density, 1 meter long plasma for accelerator applications *Proc. PAC01* FPAH151
[110] Rosenzweig J *et al* 1996 *Proc. Snowmass 1996 Workshop* http://pbpl.physics.ucla.edu/papers/PDF/NPWFA_Strawman.pdf
[111] Chen P *et al* 2001 *Proc. Adv. Acc. Concepts 9th Workshop* ed P L Colestock and S Kelley, IOP CP, vol 569, p 903
[112] Lee S *et al* 2002 *Pys. Rev* ST AB **5** 01001, http://prst-ab.aps.org/pdf/PRSTAB/v5/i1/e011001
[113] Umstadter D, Kim J K and Dodd E 1996 Laser injection of ultrashort electron pulses into wakefield plasma waves *Phys. Rev. Lett.* **76** 2073
[114] Umstadter D *et al* 2002 Laser-plasma guns and wigglers *Proc. ICFA Workshop Phys. Appl. High Brightness Electron Beams (Chia Laguna, July 2002)* http://www.physics.ucla.edu/AABD
[115] Méot F, Autin B and Verdier A 2000 A new pion collection system of the CERN neutrino factory *Proc. EPAC* MOPRI061
[116] Muon Collaboration MICE—International muon ionization cooling experiment, http://hep04.phys.iit.edu/cooldemo/
[117] Skrinsky 2000 Muon collider: basics, status, problems and prospects *Proc. Joint USA/CERN/Jp/Ru Acc. School on High Quality Beams* (AIP) p 592
[118] Ankenbrandt C M *et al* 1999 Status of muon collider R&D and future plans *Phys. Rev.* ST AB **2** 081001
[119] Autin B *et al* 2002 The study of a European neutrino factory at CERN, CERN NuFact Note 103, http://molat.home.cern.ch/molat/neutrino/nfnotes.html